AD

USAAMRDL TECHNICAL REPORT 72-7

A THEORETICAL ANALYSIS OF THE TIP RELIEF EFFECT ON HELICOPTER ROTOR PERFORMANCE

By

John M. LeNard

August 1972

EUSTIS DIRECTORATE
U. S. ARMY AIR MOBILITY RESEARCH AND DEVELOPMENT LABORATORY
FORT EUSTIS, VIRGINIA

CONTRACT DAAJ02-71-C-0006
AEROPHYSICS COMPANY
WASHINGTON, D. C.

43

DISCLAIMERS

The findings in this report are not to be construed as an official Department of the Army position unless so designated by other authorized documents.

When Government drawings, specifications, or other data are used for any purpose other than in connection with a definitely related Government procurement operation, the United States Government thereby incurs no responsibility nor any obligation whatsoever; and the fact that the Government may have formulated, furnished, or in any way supplied the said drawings, specifications, or other data is not to be regarded by implication or otherwise as in any manner licensing the holder or any other person or corporation, or conveying any rights or permission, to manufacture, use, or sell any patented invention that may in any way be related thereto.

Trade names cited in this report do not constitute an official endorsement or approval of the use of such commercial hardware or software.

DISPOSITION INSTRUCTIONS

Destroy this report when no longer needed. Do not return it to the originator.

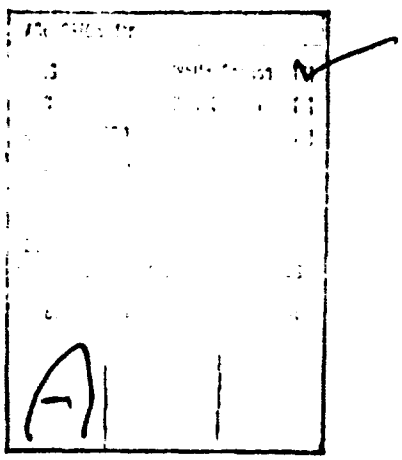

UNCLASSIFIED
Security Classification

DOCUMENT CONTROL DATA - R & D

(Security classification of title, body of abstract and indexing annotation must be entered when the overall report is classified)

1. ORIGINATING ACTIVITY (Corporate author) Aerophysics Company Washington, D.C.	2a. REPORT SECURITY CLASSIFICATION UNCLASSIFIED 2b. GROUP

3. REPORT TITLE

A THEORETICAL ANALYSIS OF THE TIP RELIEF EFFECT ON HELICOPTER ROTOR PERFORMANCE

4. DESCRIPTIVE NOTES (Type of report and inclusive dates)
Final Report

5. AUTHOR(S) (First name, middle initial, last name)
John M. LeNard

6. REPORT DATE	7a. TOTAL NO. OF PAGES	7b. NO. OF REFS
August 1972	82	56

8a. CONTRACT OR GRANT NO. DAAJ02-71-C-0006 b. PROJECT NO. 1F162204AA4201 c. d.	9a. ORIGINATOR'S REPORT NUMBER(S) USAAMRDL Technical Report 72-7 9b. OTHER REPORT NO(S) (Any other numbers that may be assigned this report) Aerophysics Company Report AR53

10. DISTRIBUTION STATEMENT

Approved for public release; distribution unlimited.

11. SUPPLEMENTARY NOTES	12. SPONSORING MILITARY ACTIVITY
	Eustis Directorate U.S. Army Air Mobility R & D Laboratory Fort Eustis, Virginia

13. ABSTRACT

A theoretical method is derived whereby the effect of the compressible three-dimensional relief on the torque required for a helicopter rotor may be calculated. The complementary wing approach is used to represent the relief effect. The effect of the wing which complements a finite wing to make it an infinite wing may be found as a reduction in the free-stream velocity. This approach was applied to fixed wings by Anderson and is extended here for application to helicopter rotors. By using a simplified blade element analysis, the magnitude of the change in torque due to tip relief has been calculated and compares well with test results. The method to use the tip relief calculation in more complex blade element computer programs is described.

DD FORM 1 NOV 68 1473 REPLACES DD FORM 1473, 1 JAN 64, WHICH IS OBSOLETE FOR ARMY USE.

UNCLASSIFIED
Security Classification

14 KEY WORDS	LINK A		LINK B		LINK C	
	ROLE	WT	ROLE	WT	ROLE	WT
Rotary wing						
Helicopter performance						
Three-dimensional flow						
Compressible flow						
Tip relief						
Wing theory						
Aspect ratio						

14

850-2-72

DEPARTMENT OF THE ARMY
U. S. ARMY AIR MOBILITY RESEARCH & DEVELOPMENT LABORATORY
EUSTIS DIRECTORATE
FORT EUSTIS, VIRGINIA 23604

This report has been reviewed by the Eustis Directorate, U. S. Army Air Mobility Research and Development Laboratory and is considered to be technically sound.

The purpose of this effort was to determine if a theoretical method for calculating the tip relief effect for fixed wings could be extended to helicopter rotors. The fixed-wing method was developed by G. F. Anderson and was published in the Journal of Aeronautical Sciences. The tip relief was further investigated for application in rotor performance calculations.

This program was conducted under the technical management of Mr. Paul H. Mirick of the Aeromechanics Division of this Directorate.

Task 1F162204AA4201
Contract DAAJ02-71-C-0006
USAAMRDL Technical Report 72-7
August 1972

A THEORETICAL ANALYSIS OF THE TIP RELIEF EFFECT ON HELICOPTER ROTOR PERFORMANCE

Final Report

Aerophysics Company Report AR-53

By

John M. LeNard

Prepared by

Aerophysics Company
Washington, D. C.

for

EUSTIS DIRECTORATE
U. S. ARMY AIR MOBILITY RESEARCH AND DEVELOPMENT LABORATORY
FORT EUSTIS, VIRGINIA

ABSTRACT

A theoretical method is derived whereby the effect of the compressible three-dimensional relief on the torque required for a helicopter rotor may be calculated. The complementary wing approach is used to represent the relief effect. The effect of the wing which complements a finite wing to make it an infinite wing may be found as a reduction in the free-stream velocity. This approach was applied to fixed wings by Anderson[1] and is extended here for application to helicopter rotors. By using a simplified blade element analysis, the magnitude of the change in torque due to tip relief has been calculated and compares well with test results. The method to use the tip relief calculation in more complex blade element computer programs is described.

FOREWORD

This investigation was sponsored by the Eustis Directorate, U.S. Army Air Mobility Research and Development Laboratory, under Contract DAAJ02-71-C-0006, Task 1F162204AA4201, during the period from October 1970 to October 1971.

The basic concept underlying this investigation was suggested by Mr. James P. Trant, Jr., Eustis Directorate, USAAMRDL, whose continued assistance during the program is gratefully acknowledged. Appreciation is expressed to Dr. Gabriel D. Boehler for the guidance provided during the investigation. Also acknowledged are the detailed notes and program decks made available by Mr. Robert Sopher. Further, a limited distribution paper[21] was made available by the Douglas Aircraft Company, McDonnell Douglas Corporation. The technical representative of the Contracting Officer for this contract was Mr. Paul Mirick.

TABLE OF CONTENTS

LIST OF ILLUSTRATIONS

LIST OF TABLES

LIST OF SYMBOLS

A	Defined in equation (2), area
a	Speed of sound
a_c	Defined in equation (112)
b	Number of blades
c	Semichord
C_D	Drag coefficient
C_p	Pressure coefficient
D	Drag, distance
F	z-coordinate of wing or blade surface
$\bar{G}_x$	Correction factor
G	Defined in equation (4)
H_c	Defined in equation (23a)
H	Defined in equation (19)
h_n	Defined in equation (25)
I_n	Defined in equation (26)
k	Source of strength
ℓn	Logarithm to the base e
M	Mach number
p	Pressure
q	Dynamic pressure
R	Total radius of a blade
r	Radial station
$\bar{r}$	Nondimensional radial station
Re	Reynolds number

t	Semithickness
U_∞	Free-stream velocity
$\vec{V}$	Velocity vector
v_x, v_y, v_z	Velocity components in Cartesian coordinates
v_θ, v_r, v_z	Velocity components in cylindrical coordinates
x,y,z	Coordinate system (see Figure 1)
β	Prandtl-Glauert factor
γ	Ratio of specific heats
ζ,η,ξ	Auxiliary coordinate system
λ	Aspect ratio
μ	Advance ratio
δ_A	Ratio of area of airfoil profile and of enclosed rectangle
δ_I	Ratio of moment of inertia of airfoil profile and of enclosed rectangle
ρ	Density
σ	Blade solidity
τ	Thickness ratio
ϕ	Potential function, inflow angle

SUPERSCRIPTS

$(\bar{})$	Averaged
$(\,)'$	Derivative, auxiliary coordinate, nondimensional

SUBSCRIPTS

$(\,)_x$	Differentiation with respect to x
$(\,)_\infty$	Condition in the undisturbed stream
$(\,)_i$	Incompressible

$( )_{eff}$	Effective
$( )_{FW}$	Finite wing
$( )_{SI}$	Semi-infinite wing
$( )_{\xi}$	Differentiation with respect to the auxiliary variable ξ
$( )_{c}$	Chord, compressible
$( )_{y}$	Refers to local value

INTRODUCTION

The present methods of calculating the performance of helicopter rotors in the compressible regime are not quite satisfactory. These methods are based on the use of two-dimensional compressible airfoil data inserted into strip element analyses and predict power losses higher than are actually found from flight test data.

Though only one of many complex factors, a prime reason for this discrepancy is the tip relief effect, i.e., the reduction in the drag of a finite body when compared to a similar body of infinite span, due to the reduction in local velocity near the tip. The existence of the tip relief effect has been well documented for both fixed and rotary wings, and the documentation indicates that the tip relief effect becomes more important as Mach number increases in the subsonic range. For the case of a wing in uniform flow, theoretical work exists which quantifies the tip relief effect. Further, a theory exists by which the drag coefficients of wings of differing aspect ratios, up to high subsonic speeds, may be correlated by a similarity law developed by Anderson.[1]

The purpose of the work reported herein was to investigate whether Anderson's work on the tip relief effect for fixed wings could be extended to rotating wings, either by a transformation of coordinates from uniform to rotating flow, or by setting up the problem directly in rotating coordinates. The approach was suggested by Trant[2] several years ago. The nonlifting finite wing is represented as a source distribution, and the actual wing is found to be mathematically equivalent to the superposition of a wing of infinite aspect ratio and of a "complementary wing" that would extend from the tip of the actual wing to infinity; the problem is initially set up for incompressible flow and then transformed into a compressible flow problem.

Early in the investigation, it was found, exactly as theorized earlier by Trant, that Anderson's method could be used for rotating wings by using a different method of averaging locally induced velocities over the wing due to the tip effect. While Anderson finds a unique correction factor for the free-stream velocity, one can find a spanwise varying correction factor, which can be used in the blade element performance analysis of rotors. Only recently, however, has a full understanding of the problem been reached, after (1) the mathematical transformation of the problem from fixed to rotating coordinates was accomplished and (2) a solution of the problem directly in rotating coordinates was attempted. The limits of validity of the solution indicated above have been established, and it has been shown that the Trant approach is correct for helicopter rotors; in addition, there is strong evidence that the mathematical formulation of the Anderson problem directly in rotating coordinates is fruitless. Limited comparisons of flight test data with a simplified blade element analysis incorporating the tip relief effect derived theoretically in the report show very encouraging correlation trends.

This report presents a detailed mathematical formulation of the tip relief effect on helicopter rotors. The report first discusses the background to the problem; then the calculation of the spanwise varying correction factor to quantitatively determine the three-dimensional relief effect is given. Whenever possible, the discussion and the derivation are in terms of fixed coordinates, as it is simpler to grasp physically and because the relationships between fixed and rotating coordinates are straightforward as is shown later in this report. Next, the basic fluid dynamic equations of a rotor are discussed, including the derivation of the small perturbation equations for subsonic and transonic flows to show the relation between compressible and incompressible flows over rotors. The source-sink distribution method of representing a rotating blade is discussed.[3] Then, use of the tip relief correction factor for compressible flow over a rotor in blade element analysis is derived. The final chapters make a comparison with experiment, discuss the results, and give conclusions and recommendations.

BACKGROUND

ROTARY-WING PERFORMANCE CALCULATIONS

Performance prediction techniques for rotary wings are highly iterative. Calculations for a single point on a performance curve may take a considerable time on a high-speed computer using one of the more sophisticated free-wake techniques. This is clearly unacceptable for preliminary design purposes, and thus methods which are reasonably simple in application, but not necessarily exact in the mathematical sense, are needed.

The two approaches to rotary-wing performance calculations are the actuator disc and the blade element theories. Since actuator disc theory assumes an infinite number of blades, it gives no information as to how the blades should be designed and ignores profile drag. Thus it is necessary to use blade element theory, which assumes that each element can be considered aerodynamically as an independent two-dimensional airfoil segment. The local forces are calculated from the resultant velocities at the element, and total forces are found by integrating the contribution of each element along the radius and the azimuth. From these forces, the motion of the blade is determined, but the motion in turn has an effect on the local velocities and thus the local angles of attack. This iteration may be avoided only by making such further assumptions as averaging the induced velocities and assuming a constant drag coefficient as is done in chapter 8 of the book by Gessow and Myers.[4] With the use of high-speed computers, the blade element iteration is used. Some of the basic assumptions used in the analysis and some of the suggested improvements include [for a more thorough review, see Gessow and Myers[4](page 198-216), Harris et al.,[5] and Bellinger[6]]:

- The use of two-dimensional steady airfoil data is almost universal. The use of so-called synthesized data has been suggested and will be discussed later in this report. There are also attempts to include unsteady stall hysterisis in the data,[6] in addition to theoretical work in the area of dynamic stall.[7]

- Tip effects are accounted for as a loss in the lifting capability of a small percentage of the blade near the tip. Often, it is simply taken as a constant B=0.97, but it can be calculated as a function of thrust coefficient based on vortex theories developed by Prandtl and Betz, as explained by Glauert[8] (page 261-269).

- The radial component of the velocity at an element is neglected, and the analysis is based only on the velocity normal to the blade span. A means of removing this limitation has been suggested by Harris,[5] based on ideas of swept-wing aerodynamics.

- The induced velocity is in many cases assumed constant. The major problem is the prediction of the location of the trailing vortices.

In fixed-wing aerodynamics, the trailing vortices are assumed to trail aft in the direction of the free-stream velocity. On a rotor, the trailing vortices are in more or less the shape of a helical sheet, due to rotation and to the nonuniform lift distribution. The helical shape for the trailing vortices was first used by Goldstein.[9] But the helical shape gives rise to a great deal of interference which distorts the wake, as described, for example, by Landgrebe.[10,11]

- Compressibility effects are taken into account by using airfoil data from two-dimensional compressible flow tests as discussed below.

The complexity of the rotating wing problem is such that only recently has any real progress been made in the basic theory. In fact, Sears[12] indicated that the blade element approach is valid. Only in December 1970 was it shown[13] that Sears is not necessarily valid for a finite span rotating blade. Boundary layer calculations (such as that by Hicks and Nash[14] and Clark and Arnoldi[15]) use the two-dimensional pressure distribution suggested by blade element analysis as the external flow. Unfortunately, very little of the basic theoretical analysis is of direct use in the design and performance prediction of rotor systems.

COMPRESSIBILITY EFFECTS ON ROTORS

Some of the approaches to account for the compressible flow over helicopter rotors will be reviewed. In the early 1950's, two basic theoretical approaches to compressibility were made. The first was solutions to the actuator disc problem in compressible flow.[16,17,18] This was combined with blade element theory by Laitone[19] for use with helicopters, The other approach by Head,[20] was the use of the Prandtl-Glauert rules for the lift coefficient variation with Mach number in a simplified blade element analysis. By including a linear decrease in lift above the lift divergence Mach number to extend the validity, the ratio of compressible-to-incompressible thrust coefficients and the ratio of induced and total torque coefficients for compressible and incompressible flows are found. Neither of these approaches recieved much use. The actuator disc theory was not used because it does not give any details concerning the airfoil design; Head's report received little circulation; and the use of two-dimensional compressible airfoil data in blade element analysis was begun at the same time.

Airfoil data obtained in two-dimensional compressible flow in blade element analysis were used to find the effects of compressibility and to make corrections to the available incompressible rotor charts. Typically, these were numerically integrated by calculators and made a large number of assumptions.[21,22] The culmination of this effort is the charts and tables prepared by Tanner,[23,24] using a highly sophisticated computer program with airfoil data from "two-dimensional wind tunnel tests of a production blade specimen using the NACA 0012 airfoil section".

The inconsistency of using two-dimensional data in rotating airfoil problems first came to light during propeller tests.[25] The drag divergence tip Mach number of a propeller was found to be about 0.06 above the two-dimensional result, and performance tests of full-scale helicopter rotors in hover indicated the same trend.[26] Therefore, Carpenter[27,28] proposed the use of "synthesized" airfoil data, which are obtained by "adjusting the airfoil data in such a manner that the calculated performance agrees closely with the measured performance". He stated further on page 2 of Reference 28 that "although the synthesized data are derived from rotor hovering performance, it can be reasonably assumed (until proven otherwise) that the data are equally applicable to forward flight calculations". Charts similar to Tanner's were prepared by Kisielowski et al.,[29] using the synthesized data of Reference 28, but these latter charts appear to be rarely used. It would be of interest to compare the predicted performance using each of the two sets of charts with some actual flight test data.

The problem of helicopters at high forward speeds is that compressibility effects and stall occur at the same time on the rotor. At the advancing tip, the forward speed and the rotational speeds add, resulting in speeds of approximately Mach one. But on the retreating side the two speeds subtract, resulting in a region of reverse flow and areas where the flapping blades are at or above the stall angle of attack. The dividing line between stall losses and compressibility losses is not indicated by test data,[26] and both areas must be taken into account in rotor analysis.

To reduce the data and decrease the amount of flight test required, personnel at the Edwards AFB Flight Test Center have been developing an approach, mainly empirical, to account for compressibility effects.[30-33] Drawing on fixed-wing experience, the power required is divided into two portions: (1) the incompressible power; and (2) an increment in power due to compressible flow, which depends on the difference between the critical Mach number of the blade section and the Mach number of the element. The correlation is established empirically using UH-1F and CH-47A flight test data.[30,31] Later reports[32,33] include the effects of power losses due to retreating blade stall.

Another approach[34] to the aerodynamic problem of a rotor blade in compressible flow has been taken by Bell Helicopter Company in its design of the Model 309 King Cobra. The rotor system embodies an asymmetrical airfoil section and a double swept tip. The airfoil section designed by Prof. Wortman[35] is based on the aerodynamic requirements for two-dimensional airfoils found from basic blade element theory. Swept wings have long been used to delay the effects of compressibility on fixed-wing aircraft. Similar sweeping of the leading edge of the blade tip will reduce compressibility effects in forward flight.[36]

Thin blades near the tips to reduce the drag divergence Mach number have also been considered by Bell.[36] But in uniform flows, a thin airfoil has a lower maximum lift coefficient and stalls at a lower angle of attack, which in a rotor would increase the power on the retreating side. The Sikorsky S-67 Blackhawk also incorporates the sweeping and a thinner section of the blade tip to reduce compressible flow effects.

Surprisingly, though, full-scale wind tunnel tests[37] indicate that the lifting capability of a thin-tipped bladed rotor is not compromised, while it requires significantly less power at high advancing tip Mach numbers than a blade with constant thickness.

THE THREE-DIMENSIONAL RELIEF EFFECT ON ROTORS

This report is concerned with one aspect of the rotor compressibility problem. As noted above, two-dimensional airfoil data overestimate the compressibility losses. One possible factor may be the reduction in drag coefficient of a finite wing in compressible flow compared to a similar two-dimensional airfoil. As will be described, this relief effect may be determined in a quantitative manner and applied to the performance calculation of rotary wings.

In a three-dimensional flow, the stream may deviate from the main stream in both directions perpendicular to the body chord line. At the same time, in two-dimensional flow, only deviation in the direction perpendicular to both the chord and the span is possible. Therefore, lesser disturbances are produced by three-dimensional bodies than by two-dimensional bodies. (See the discussion of Figure 10.) This reduction in disturbance velocity is also a reduction in Mach number, and thus a reduction in critical Mach number.

That this disturbance reduction in a three-dimensional flow increases with free-stream Mach number was found[38] analytically for flow past ellipsoids of various aspect ratios; the difference between the maximum velocity of an elliptic cylinder (an ellipsoid of infinite aspect ratio) and a finite aspect ratio ellipsoid was found to increase with Mach number (see, for example, Figure 13-2 of Shapiro's book,[39]) On airplane wings of normal aspect ratio at incompressible speeds, the wing is considered to be two-dimensional. The effect of aspect ratio is found from the Prandtl lifting line theory as an additional angle of attack and an induced drag due to the effect of the trailing vortices. The induced drag of the wing is found to vary inversely as the aspect ratio.

Goethert[40] extended the Prandtl-Glauert transformation between compressible and incompressible flows to finite wings. The result is that, instead of the simple affine transformation of a two-dimensional body to reduce it to an equivalent incompressible flow, for a three-dimensional body all lateral dimensions must be reduced by the amount $\beta = \sqrt{1 - M^2}$. For a more detailed discussion, see Shapiro,[39] article 13-2, and Jones and Cohen,[41] pages 48-52.

But at higher speeds, not only the lift but the drag of the wing is affected by aspect ratio, and the Goethert extension does not account for the three-dimensional relief effect. Therefore, a means to quantitatively predict the relief effect is needed. Anderson[1] developed a theory for the relief effect on fixed wings in the nonlifting case. This theory is extended here and is applied to rotary wings.

Anderson's theory for the tip relief used a "complementary wing" approach, the complementary wing being a fictitious wing extending from the actual wing tip to infinity on either side. His basic proposition is that the velocity at the location of a finite wing can be considered to be the same as for the infinite wing, reduced by the amount which would have been contributed by portions of the infinite wing that were removed from the flow (the complementary wings). These values can be calculated by linearized, subsonic compressible flow theory, using a source-sink distribution to represent the thickness effect of a symmetrical wing. In the case of the fixed wing considered by Anderson, the effect of the complementary wing can be averaged over the planform area of the finite wing, resulting in a "correction factor" which is a function of aspect ratio but not of position. The application of this correction factor is "that the finite wing will be considered to experience the same static pressure to total pressure ratio at corresponding points as the infinite wing, but only when measured at a free-stream velocity which is greater, by the correction (factor) calculated, than the free-stream velocity over the infinite wing". In other words, we can make use of two-dimensional airfoil information in the calculation of three-dimensional flows through the use of the correction in free-stream velocity. This will be explained in more detail in the chapters which follow.

THE TIP RELIEF EFFECT

A quantitative means to calculate the tip relief effect, so that it may be applied to rotary wings, is derived in this section. The derivation will follow the concept and the treatment proposed by Anderson.[1] The major difference between Anderson's reports and this report is that Anderson, being interested in fixed wings, intended to obtain the correction as a function of aspect ratio λ alone, while here it is necessary to obtain results as function of aspect ratio and distance from the tip, so that it may be applied to rotors.

The result which will be obtained here and that found by Anderson is that two-dimensional results, be they from theory, wind tunnel or flight test data, may be used, through the transformation derived here, in the calculation of three-dimensional flows.

The discussion here will be concerned with a wing in a subsonic uniform airflow with a constant airfoil section. The flow is assumed to be subcritical, with no shock waves, and inviscid without separation. The airfoil is assumed to be thin; thus the thickness of the airfoil may be represented by the linear theory distribution of sources and sinks, namely, that the source-sink distribution is proportional to the local streamwise slope of the airfoil. Although this is invalid at the leading and trailing edges, because of the averaging process which will be discussed below, no correction needs to be made. The discussion is further restricted to the nonlifting case, i.e., the effect of thickness only. It is believed that the major cause of tip relief is thickness, rather than angle of attack or camber.

The derivation will be made for a wing in uniform flow, as the physical characteristics can be most easily explained and the equations are more familiar. At the end of this section it will be shown that the result is the same for the rotating case as may be expected from the theory developed by Sears.[12]

The Goethert extension of the Prandtl-Glauert rule is used in the analysis for application to fixed wings. The factor $\beta^2 = 1 - M^2$ will be used to transform between the compressible flow and the equivalent incompressible flow, rather than any of the higher order developments. Extra complexities of the higher order theories are not justified for this application. Further extension to rotary wings is discussed in the next chapter.

PHYSICAL AND MATHEMATICAL MODELS FOR THE TIP RELIEF EFFECT

Consider a symmetrical airfoil wing in inviscid, incompressible flow at zero angle of attack. Due to the principle of superposition, the velocity at any point is the sum of the free-stream velocity and the velocity induced by the wing. The induced velocity of a finite span wing may be represented by a source-sink distribution over the planform area of the wing. But

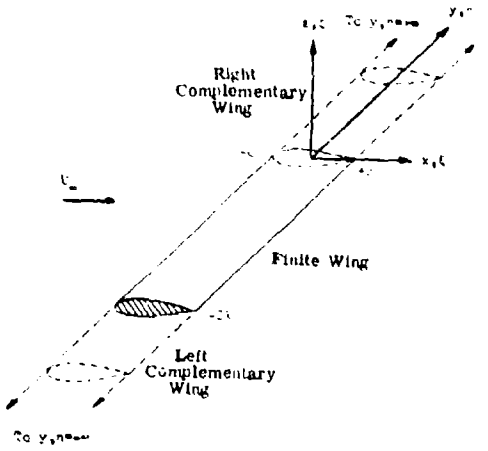

Figure 1. Coordinate System for a Finite Wing.

because of superposition, the finite span wing may also be represented by a similar infinite span wing less "complementary wings". The complementary wing is a similar wing extending from the tips of the finite wing to infinity on both sides. The concept of the complementary wing is illustrated in Figure 1 for a wing of chord 2c and span of 2λ. We may write this discussion in equation form as

$$\phi = U_\infty x + \int_{-2\lambda}^{0} U_\infty A \, d\eta \qquad (1)$$

for the potential of a finite wing of aspect ratio λ, with flow along the x-axis and origin at the right wing tip, where A represents the source-sink distribution integral

$$A = -\frac{1}{2\pi} \int_{-c}^{+c} \frac{F_\xi(\xi) \, d\xi}{\sqrt{(x-\xi)^2 + (y-\eta)^2 + z^2}} \qquad (2)$$

where the subscript ξ indicates differentiation. This coordinate system was chosen so that it may later correspond to a helicopter rotor.

The potential of the finite wing using a pair of complementary wings is

$$\phi = U_\infty x + \int_{-\infty}^{+\infty} U_\infty A \, d\eta - \int_{-\infty}^{-2\lambda} U_\infty A \, d\eta - \int_{0}^{+\infty} U_\infty A \, d\eta \qquad (3)$$

The values of φ obtained from either equation (1) or (3) have to be identical.

The first integral in equation (3) (with limits of plus and minus infinity) is simply the potential of an infinite or two-dimensional airfoil, and thus can be represented by the symbol $\phi_{\lambda=\infty}$.

The last two integrals give values which vary with position throughout the flow field. If an average value of these two terms can be obtained, the problem becomes greatly simplified. Let

$$G(\lambda, x, y, z) = \int_{-\infty}^{-2\lambda} A \, d\eta + \int_{0}^{\infty} A \, d\eta \qquad (4)$$

Then equation (3) becomes

$$\phi = U_\infty x + \phi_{\lambda=\infty} - U_\infty G(\lambda, x, y, z) \tag{5}$$

The velocity in the streamwise direction may be simply written from equation (5) as

$$u = \frac{\partial \phi}{\partial x} = U_\infty + u_{\lambda=\infty} - U_\infty G_x \tag{6a}$$

or

$$u = U_\infty (1 - G_x) + u_{\lambda=\infty} \tag{6b}$$

which may also be written as

$$\frac{du}{U} = -G_x \tag{6c}$$

If an averaged value of G_x can be found (denoted by $\bar{G}_x$), then the velocity on the finite wing u can be compared to the velocity of an infinite wing, but at the new free-stream velocity of $U_\infty(1-\bar{G}_x)$. Therefore, the finite wing will experience the same static pressure to total pressure ratio at corresponding points as the infinite wing at a free-stream velocity, which is greater than the free-stream velocity of the infinite wing by the correction $\bar{G}_x$. Therefore, the finite and the infinite wing will experience the same force per unit span when

$$U_\infty(1-\bar{G}_x) \Big|_{\substack{\text{finite} \\ \text{wing}}} = U_\infty \Big|_{\substack{\text{infinite} \\ \text{wing}}} \tag{7}$$

holds for the free-stream velocity.

The correction $\bar{G}_x(\lambda)$ was found by Anderson[1] by averaging over the planform area of finite wing

$$\bar{G}_x(\lambda) = \frac{1}{2c}\,\frac{1}{2\lambda} \int_{-c}^{+c} \int_{-2\lambda}^{0} G_x(\lambda, x, y, z)\,dx\,dy \tag{8}$$

If instead the averaging is done only over the chord of the finite wing, then a correction will be obtained which will be a function of aspect ratio λ and span y,

$$\bar{G}_x(\lambda, y) = \frac{1}{2c} \int_{-c}^{+c} G_x(\lambda, x, y, z)\,dx \tag{9}$$

With the correction as a function of spanwise position, it becomes applicable to a rotary wing where there are major spanwise variations.

The variable z, in the airfoil thickness direction, is eliminated since the wing is assumed to be in the z = 0 plane.

THE CORRECTION FOR A SEMI-INFINITE WING

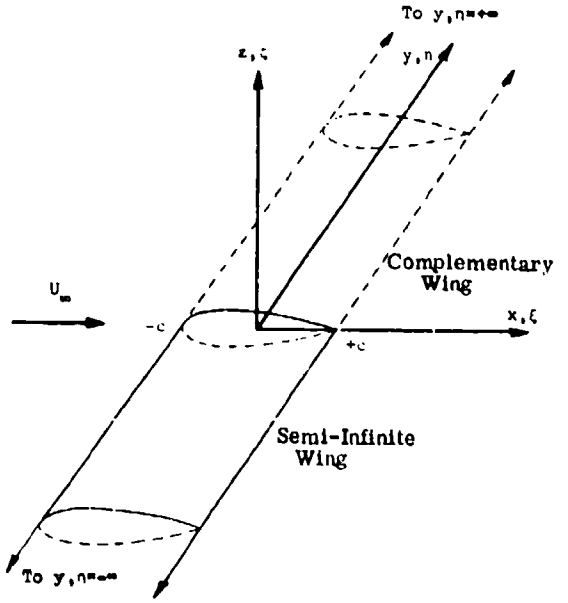

Figure 2. Coordinate System for a Semi-Infinite Wing.

The main effect of a complementary wing will be felt near the tip where the complementary wing joins the finite wing, rather than at the opposite wing tip. Thus a further simplification may be found if the complementary wing opposite to the tip under consideration is neglected. The problem may then be posed as the complementary wing of a semi-infinite wing (see Figure 2). Mathematically, this removes the first term of equation (4). In this section the correction for the semi-infinite wing will be derived, while in the next two sections the correction for a finite wing is derived, and then the two corrections are compared.

Mathematically, the problem is the substitution of equation (2) for A into equation (4) for the complementary wing potential and then in turn into equation (9) for the correction, and carrying out the indicated mathematical operations. The complementary wing potential for a semi-infinite wing is, from equations (2) and (4),

$$G(x,y,z) = -\frac{1}{2\pi} \int_0^{\infty} \int_{-c}^{+c} \frac{F_\xi(\xi)\, d\xi\, d\eta}{\sqrt{(x-\xi)^2 + (y-\eta)^2 + z^2}} \qquad (10)$$

Taking the derivative of G with respect to x results in

$$G_x = \frac{\partial G}{\partial x} = \frac{\partial}{\partial x} \int_0^{\infty} \int_{-c}^{+c} \frac{-1}{2\pi} \frac{F_\xi(\xi)\, d\xi\, d\eta}{\sqrt{(x-\xi)^2 + (y-\eta)^2 + z^2}}$$

$$= \frac{1}{2\pi} \int_0^{\infty} \int_{-c}^{+c} \frac{F_\xi(\xi)\,(x-\xi)\, d\xi\, d\eta}{\left\{(x-\xi)^2 + (y-\eta)^2 + z^2\right\}^{3/2}} \qquad (11)$$

The integration with respect to η over the span ($0<\eta<\infty$) of the complementary wing through the use of integral form Petit Bois 67-14[42]*

$$\int \frac{du}{(A^2 + u^2)^{3/2}} = \frac{u}{A^2 \sqrt{A^2 + u^2}} \tag{12}$$

where $u = y - \eta$
$du = - d\eta$
$A^2 = (x-\xi)^2 + z^2$

and $F_\xi(\xi)$ is constant with respect to the integration. Noting that the upper limit of integration is

$$\lim_{u \to -\infty} \frac{u}{\sqrt{A^2 + u^2}} = \frac{-\infty}{\infty} = -1$$

results in

$$G_x = \frac{1}{2\pi} \int_{-c}^{+c} F\xi\ (x-\xi)\ d\xi \int_{y}^{y=\infty} \frac{-du}{(A^2 + u^2)^{3/2}}$$

$$G_x = \frac{-1}{2\pi} \int_{-c}^{+c} \frac{F_\xi (x-\xi) d\xi}{(x-\xi)^2 + z^2} \left[\frac{y}{\sqrt{(x-\xi)^2 + y^2 + z^2}} + 1 \right] \tag{13}$$

Substituting into equation (9) to obtain the average chordwise correction,

$$\bar{G}_x(y) = \frac{-1}{4\pi c} \int_{-c}^{+c} \int_{-c}^{+c} \frac{F_\xi (x-\xi)}{(x-\xi)^2 + z^2} \left[\frac{y}{\sqrt{(x-\xi)^2 + y^2 + z^2}} + 1 \right] d\xi\ dx \tag{14}$$

Evaluating at the chord line, $z = 0$, equation (14) simplifies to

$$\bar{G}_x(y) = \frac{-1}{4\pi c} \int_{-c}^{+c} \int_{-c}^{+c} \frac{F_\xi}{(x-\xi)} \left[\frac{1}{\sqrt{(x-\xi)^2 + y^2}} + 1 \right] d\xi\ dx \tag{15}$$

* Petit Bois 67-14 indicates the 14th integral form given in Reference 42 on page 67.

Equation (15) may be integrated with respect to x holding F_ξ as a constant, since F_ξ is a function of the auxiliary coordinate ξ. The use of integral forms Petit Bois 1-4 and 45-10 results in the following equation:

$$\bar{G}_x(y) = \frac{-1}{4\pi c}\int_{-c}^{+c} F_\xi \left[y \int_{-c}^{+c} \frac{dx}{(x-\xi)\sqrt{(x-\xi)^2 + y^2}} + \int_{-c}^{+c} \frac{dx}{(x-\xi)} \right] d\xi$$

$$= \frac{-1}{4\pi c}\int_{-c}^{+c} F_\xi \left[y \frac{1}{y} \ln \frac{\sqrt{u^2 + y^2} - y}{u} \Bigg|_{-(c+\xi)}^{c-\xi} + \ln u \Bigg|_{-(c+\xi)}^{c-\xi} \right] d\xi$$

$$\bar{G}_x(y) = \frac{-1}{4\pi c}\int_{-c}^{+c} F_\xi(\xi) \left[\ln \frac{1 + \sqrt{\left(\frac{c-\xi}{y}\right)^2 + 1}}{1 + \sqrt{\left(\frac{c+\xi}{y}\right)^2 + 1}} \right] d\xi \qquad (16)$$

To evaluate equation (16) further, a specific airfoil under consideration must be given and its slope F_ξ inserted into equation (16) before carrying out the integration. An attempt was made to carry out this integration for an airfoil whose thickness is given by a simple algebraic series, such as the NACA four-digit series, without success. Two other approaches were used successfully to evaluate the integral of equation (16). The first is numerical integration, while the second is a Taylor series expansion which results in a simple but accurate approximate equation of wide application.

Numerical Integration

Numerical integration of equation (16) was made using Simpson's rule in a computer program. This, of course, requires an even spacing of intervals. In most instances, 30 intervals were used with the upper and lower limits $\pm$ 0.9999c to avoid possible singularities and division by zero within the computer. To indicate the accuracy with the number of intervals, Table I compares the values of $\bar{G}_x$ using 20 and 30 terms for a parabolic arc airfoil.

TABLE I. COMPARISON OF INTEGRAL ACCURACY WITH NUMBER OF TERMS

Span Position y/c	Semi-Infinite, Parabolic Arc Wing	
	20 terms	30 terms
$0.10_{\hat{a}}$	-0.02184	-0.02226
0.50	-0.01041	-0.01058
1.00	-0.00528	-0.00537
3.00	-0.00098	-0.00101

Differences in the final change in torque due to the number of terms are even smaller than indicated in the table.

Further discussion of results will be in comparison with other methods of evaluating equation (16).

Taylor Series Approximation

If the bracketed term of equation (16) is expanded in a Taylor series of ξ, the airfoil slope F_ξ will then appear in integrals of the form

$$\int_{-c}^{+c} F_\xi(\xi)\xi^n d\xi \tag{17a}$$

which, as will be shown later, may be further reduced to

$$\int_{-c}^{+c} F(\xi)\xi^m d\xi \tag{17b}$$

Anderson found[1] that for the usual airfoil section, the values of these integrals cannot have large variations.

Therefore, we can write equation (16) as

$$\bar{G}_x = \frac{1}{4\pi c} H_o(c/y) + \frac{1}{4\pi c} H_1'(c/y) \int_{-c}^{+c} F_\xi \xi d\xi + \ldots + \frac{H_n^{n'}(c/y)}{4\pi c\, n!} \int_{-c}^{+c} F_\xi \xi^n d\xi \qquad (18)$$

where

$$H(\xi) = \ln \frac{1 + \sqrt{((c-\xi)/y)^2 + 1}}{1 + \sqrt{((c+\xi)/y)^2 + 1}} = H_o + \xi H' \ (c/y, \xi = 0)$$

$$+ \ \ldots + \frac{1}{n!} \xi^n H^{n'}(c/y, \ \xi = 0) \qquad (19)$$

where

$$H^{n'} = \frac{\partial^n H}{\partial \xi^n} \qquad (20)$$

The integrals of equation (18) will be discussed in a later section on the effect of airfoil section, while here the first three nonzero terms of the Taylor series of equation (19) will be given.

For the Taylor series, the derivatives of the logarithm terms, which are of the form

$$\ln(1 + \sqrt{p^2 + 1}) \qquad (21)$$

are found as follows:

First Derivative

$$\frac{d}{d\xi}(\ln (1 + \sqrt{p^2 + 1})) = \frac{1}{\sqrt{p^2 + 1} + 1} \frac{1}{2} \frac{2p}{\sqrt{p^2 + 1}} p'$$

$$= - \frac{p'}{p} \frac{1 - \sqrt{p^2 + 1}}{\sqrt{p^2 + 1}} \qquad (22a)$$

Second Derivative

$$\frac{d}{d\xi}\left(-\frac{p'}{p}\,\frac{1-\sqrt{p^2+1}}{\sqrt{p^2+1}}\right) = -\,p'^2\,\frac{p\sqrt{p^2+1}\,\left(-p/\sqrt{p^2+1}\right)-(1-\sqrt{p^2+1})\left(p^2/\sqrt{p^2+1}+\sqrt{p^2+1}\right)}{p^2(p^2+1)}$$

$$= -\left(\frac{p'}{p}\right)^2\left[\frac{2p^2+1}{p^2(p^2+1)^{3/2}} - 1\right] \qquad (22b)$$

Third Derivative

$$\frac{d}{d\xi}\left[-\left(\frac{p'}{p}\right)^2\left(\frac{2p^2+1}{p^2(p^2+1)^{3/2}}-1\right)\right] = -\,p'^3\left[\frac{p(p^2+1)4p-(2p^2+1)\,(2(p^2+1)+3p)}{p^4(p^2+1)^3} - \frac{2}{p^3}\right]$$

$$= \left(\frac{p'}{p}\right)^3\left[\frac{6p^4+5p^2+2}{(p^2+1)^{5/2}} - 2\right] \qquad (22c)$$

Fourth Derivative

$$\frac{d}{d\xi}\left[\frac{p'^3}{p^3}\left(-\frac{6p^4+5p^2+2}{(p^2+1)^{5/2}} + 2\right)\right]$$

$$= p'^4\left(-\frac{p^3(p^2+1)^{5/2}(24p^3+10) - (6p^4+5p^2+2)\,(3p^2(p^2+1)^{5/2} + p^3 5(p^2+1)^{3/2}p)}{p^6(p^2+1)^5} - \frac{6}{p^4}\right)$$

$$= \frac{3p'^4}{p^4}\left[\frac{8p^6+8p^4+7p^2+2}{(p^2+1)^{7/2}} - 2\right] \qquad (22d)$$

Fifth Derivative

$$\frac{d}{d\xi}\left[\frac{3p'^4}{p^4}\left(\frac{8p^6+8p^4+7p^2+2}{(p^2+1)^{7/2}} - 2\right)\right] =$$

$$= 3p'^5\left[\frac{p^4(p^2+1)^{7/2}(48p^5+32p^3+14p)-(8p^6+8p^4+7p^2+2)(4p^3(p^2+1)^{7/2}+p^4 7(p^2+1)^{5/2}p)}{p^8(p^2+1)^7}+\frac{8}{p^5}\right]$$

$$= \frac{3p'^5}{p^5}\left[-\frac{40(p^8+p^6)+63p^4+36p^2+8}{(p^2+1)^{9/2}}+8\right] \tag{22e}$$

The terms of the Taylor series are then found by evaluating at $\xi = 0$. Note that there are two terms of the form of equation (21) with $p_1 = (c-\xi)/y$ and $p_2 = (c+\xi)/y$. Further note that

$$p_1' = \frac{dp_1}{d\xi} = -\frac{dp_2}{d\xi} = -p_2' = -1/y$$

First Term

$$H_0(c/y,\xi = 0) = \ln\frac{1+\sqrt{(c/y)^2+1}}{1+\sqrt{(c/y)^2+1}} = \ln 1 = 0 \tag{23a}$$

Second Term

$$H_1'(c/y,\xi = 0) = -\frac{(1/y)}{(c/y)}\frac{1-\sqrt{(c/y)^2+1}}{\sqrt{(c/y)^2+1}}+\frac{(-1/y)}{(c/y)}\frac{1-\sqrt{(c/y)^2+1}}{\sqrt{(c/y)^2+1}}$$

$$= \frac{2}{c}\left[\frac{\sqrt{(c/y)^2+1}-1}{\sqrt{(c/y)^2+1}}\right] \tag{23b}$$

Third Term

$$H_2''(c/y,\xi = 0) = -\frac{(1/y)^2}{(c/y)^2}\left[\frac{2(c/y)^2+1}{((c/y)^2+1)^{3/2}}-1\right]+\frac{(-1/y)^2}{(c/y)^2}\left[\frac{2(c/y)^2+1}{((c/y)^2+1)^{3/2}}-1\right]$$

$$H_2''(c/y,\xi = 0) = 0 \tag{23c}$$

Fourth Term

$$H'''(c/y,\xi = 0) = 4-2\frac{6(c/y)^4+5(c/y)^2+2}{((c/y)^2+1)^{5/2}} \tag{23d}$$

Fifth Term

$$H^{IV}(c/y,\xi = 0) = 0$$

Sixth Term

$$H^{V}(c/y,\xi=0) = \frac{1}{c^5}\left[48 - 6\frac{40\left[(c/y)^8 + (c/y)^6\right] + 63(c/y)^4 + 36(c/y)^2 + 8}{\left((c/y)^2 + 1\right)^{9/2}}\right] \quad (23e)$$

Therefore, the correction factor may be written in terms of a Taylor series expansion for the first three nonzero terms as

$$\bar{G}_x = (1/4\pi c)(h_1 I_1/c + h_2 I_2/c^3 + h_3 I_3/c^5) \quad (24)$$

where we have defined

$$\left.\begin{aligned} h_1 &= H'(c/y,\xi = 0) \\ h_2 &= H'''(c/y,\xi = 0)/3! \\ h_3 &= H^{V}(c/y,\xi = 0)/5! \end{aligned}\right\} \quad (25)$$

$$\left.\begin{aligned} I_1 &= \int_{-c}^{+c} F_\xi \xi d\xi \\ I_2 &= \int_{-c}^{+c} F_\xi \xi^3 d\xi \\ I_3 &= \int_{-c}^{+c} F_\xi \xi^5 d\xi \end{aligned}\right\} \quad (26)$$

THE CORRECTION FOR A FINITE WING

The derivation for a finite wing follows a very similar pattern to that presented for the semi-infinite wing. The complementary potential for a finite wing is

$$G(\lambda,x,y,z) = -\frac{1}{2\pi}\int_{+c}^{-c}\int_{-\infty}^{-2\lambda}\frac{F_\xi\, d\xi\, d\eta}{\sqrt{(x-\xi)^2 + (y-\eta)^2 + z^2}}$$

$$-\frac{1}{2\pi}\int_{+c}^{-c}\int_{0}^{\infty}\frac{F_\xi\, d\xi\, d\eta}{\sqrt{(x-\xi)^2 + (y-\eta)^2 + z^2}} \quad (27)$$

Differentiating with respect to x,

$$G_x = \frac{1}{2\pi}\int_{-c}^{+c}\int_{-\infty}^{-2\lambda} \frac{F_\xi\,(x-\xi)\,d\xi\,d\eta}{((x-\xi)^2 + (y-\eta)^2 + z^2)^{3/2}}$$

$$+\frac{1}{2\pi}\int_{-c}^{+c}\int_{0}^{\infty} \frac{F_\xi(x-\xi)\,d\xi\,d\eta}{((x-\xi)^2 + (y-\eta)^2 + z^2)^{3/2}} \qquad (28)$$

Integrating with respect to η over $(-\infty < \eta < -2\lambda)$ and $(0 < \eta < \infty)$ in the same manner as equation (13) was obtained:

$$G_x = \frac{-1}{2\pi}\int_{-c}^{+c} \frac{F_\xi}{(x-\xi)}\left[\frac{y}{\sqrt{(x-\xi)^2 + y^2}} - \frac{2\lambda-y}{\sqrt{(x-\xi)^2 + (2\lambda-y)^2}} + 2\right]d\xi \qquad (29)$$

Averaging in accordance with equation (9) and evaluating at z = 0,

$$\bar{G}_x = \frac{-1}{4\pi c}\int_{-c}^{+c}\int_{-c}^{+c} \frac{F_\xi}{(x-\xi)}\left[\frac{y}{\sqrt{(x-\xi)^2 + y^2}} - \frac{2\lambda-y}{\sqrt{(x-\xi)^2 + (2\lambda-y)^2}} + 2\right]d\xi \qquad (30)$$

Carrying out the integration in the manner used to obtain equation (16) results in

$$\bar{G}_x(y) = \frac{-1}{4\pi c}\int_{-c}^{+c} F_\xi\left[\ln\frac{1+\sqrt{u_1^2+1}}{1+\sqrt{u_2^2+1}} + \ln\frac{1+\sqrt{u_3^2+1}}{1+\sqrt{u_4^2+1}}\right]d\xi \qquad (31)$$

where

$$\left.\begin{aligned} u_1 &= (c-\xi)/y \\ u_2 &= (c+\xi)/y \\ u_3 &= (c-\xi)/(y-2\lambda) \\ u_4 &= (c+\xi)/(y-2\lambda) \end{aligned}\right\} \qquad (32)$$

We may compare equation (31) for the finite wing with equation (16) for the semi-infinite wing. As may be expected, the correction factor for the finite wing is the sum of the correction factor for a semi-infinite wing with its tip at the origin going toward positive infinity, given by the first term (u_1 and u_2) of equation (31) and another semi-infinite wing with its tip at $y = -2\lambda$, going toward negative infinity, given by the second term (u_3 and u_4) of equation (31). In a similar manner, the Taylor series expansion terms given by equations (23) are

$$H_i\Big|_{\substack{\text{finite}\\\text{wing}}} = H_i\Big|_{SI} \quad (c/y = c/y) + H_i\Big|_{SI} \quad (c/y = c/(2\lambda - y)) \tag{33}$$

where SI indicates semi-infinite wing. The forms of equations (24) and (25) will thus hold for finite wings.

AIRFOIL SECTION CHARACTERISTICS

The integrals of equation (26) may be simplified and use made of the equation for the airfoils rather than the airfoil slope, by setting up these integrals using the method of integration by parts ($\int u dv = uv - \int v du$). The first integral in equation (26)

$$I_1 = \int_{-c}^{+c} F_\xi \xi d\xi = \xi F \Big|_{-c}^{+c} - \int_{-c}^{+c} F d\xi = -\int_{-c}^{+c} F d\xi \tag{34a}$$

since

1. $F_\xi = \dfrac{dF}{d\xi}$

2. $u = \xi \qquad dv = F_\xi d\xi = \dfrac{dF}{d\xi} d\xi = dF$

   $du = d\xi \qquad v = F$

3. $F = 0$ at $\xi = \pm c$, i.e., the thickness is zero at both leading and the trailing edges.

Statements 1 and 3 will hold exactly for the other two integrals, and statement 2 will be similar with $u = \xi^n$ and $du = n\xi^{n-1} d\xi$.

$$I_2 = \int_{-c}^{+c} F_\xi \xi^3 \, d\xi = -3 \int_{-c}^{+c} F\xi^2 \, d\xi \tag{34b}$$

and

$$I_3 = \int_{-c}^{+c} F_\xi \xi^5 \, d\xi = -5 \int_{-c}^{+c} F\xi^4 \, d\xi \tag{34c}$$

The limitation on these integrals may be found from comparing the actual profile to a rectangle enclosing the profile. Comparing the areas of the rectangle and the profile,

$$2 \int_{-c}^{+c} F \, d\xi = \text{area of airfoil}$$

$$4tc = \text{area of rectangle}$$

Let

$$\delta_A = 2 \int_{-c}^{+c} F d\xi / 4tc \tag{35a}$$

then

$$-I_1 = \int_{-c}^{+c} F d\xi = \frac{1}{2} \delta_A 4tc \frac{c}{c} \frac{c}{c} = 2\delta_A \frac{t}{c} c.c \tag{35b}$$

Nondimensionalizing by defining the leading and trailing edges at $\pm$ 1 (chord length = 2, c = 1),

$$I_1 = -2\delta_A \tau \tag{35c}$$

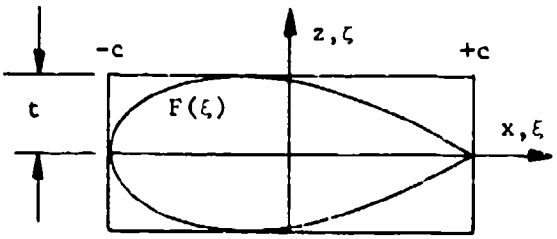

Figure 3. Geometrical Relationship.

The definiton of δ_A is the ratio of the area of the profile to the area of the rectangle. It may be seen from Figure 3 that the ratio of these two areas will not vary greatly for the usual airfoil sections. In a similar manner, the moment of inertia of the profile and the enclosing rectangle may also be compared:

$$2 \int_{-c}^{+c} F \xi^2 \, d\xi = \text{moment of inertia of the profile}$$

$$(2t)(2c)^3/12 = \text{moment of inertia of rectangle}$$

Let

$$\delta_I = \int_{-c}^{+c} 2 F \xi \, d\xi \; / \; (4tc^3/3) \qquad (36a)$$

When nondimensionalized, I_2 becomes

$$I_2 = \int_{-c}^{+c} F \xi^3 \, d\xi = - 2\delta_I \tau/3 \qquad (36b)$$

Again by inspection of Figure 3, the ratio of the moment of inertia of the profile to that of the rectangle will not vary by much. Unfortunately, there is no similar physical argument for the third integral.

The values of the integrals of equation (34) were calculated for some airfoils. Table II shows these calculated values for an airfoil approximated by an ellipse for the nose section and a parabolic arc for the rear portion (from reference 1), and a parabolic arc airfoil.

It should be pointed out that δ_A and δ_I are independent of the coordinate system and are dimensionless, while the values of the integrals do depend on the coordinate system, and the values given in the table should be used only for the case where the length is measured in terms of the semichord as is done in this report (see Figure 3.)

TABLE II. AIRFOIL CONTANT, I_n/τ		
n	Elliptic Nose Parabolic Rear	Parabolic Arc
1	-1.434	-1.333
2	-0.989	-0.80
3	-	-0.571

CHARACTERISTICS OF THE CORRECTION FACTOR

A simple computer program was written to calculate $\bar{C}_x$ so that its characteristics may be studied. The program integrated equations (16) and (31) numerically for $\bar{C}_x$ and calculated $\bar{C}_x$ as a Taylor series expansion (see equation (24) for both the finite and the semi-infinite wing). From these calculations, the plots presented in Figures 4 through 8 were made. The comparisons made in this section are for a 10% thick parabolic arc airfoil section, but the general trends will apply for other sections.

Figures 4 and 5 show the coefficients of the Taylor series for a semi-infinite wing (Figure 4) and wings of aspect ratio 2,3 and 4. The following observation may be made:

- The coefficients decrease at a fairly rapid rate near the tip.
- The first term is dominant by far over the full span.
- The second coefficient becomes negative about one-half semichord from the tip, has a negative maximum at about 0.9 semichord, and then becomes asymptotic to zero. For $y>2.25c$, the absolute value of the second coefficient is less than one-tenth of the first coefficient.
- The third coefficient is negative in the range $0.25<y/c<1.2$, with a negative maximum at about $y = 0.45c$. After becoming positive at $y/c\sim1.2$, a maximum occurs at $y/c\sim1.5$, but at this maximum the ratio of the first term to the third term is about 1/100. Above $y/c>0.1$, this term is less than one-tenth of the first term.
- The second and the third terms are more nearly equal in magnitude, and thus one should not be neglected in favor of the other.
- At the wing tip, the limiting values are:

h_1 ——————→ 2.0

h_2 ——————→ 0.667

h_3 ——————→ 0.4

- These observations hold for the three finite aspect ratios and for the semi-infinite wing. The similarities of the shapes of the curves and the magnitudes are obvious.

The correction factor $\bar{G}_x$ is shown in Figures 6, 7 and 8. Figures 6 and 7 compare the three means of calculating the correction factor:

1. using the first term of the Taylor series only

2. using the first three nonzero terms of the Taylor series

3. using a numerical integration scheme with 30 terms from -0.9999c to 0.9999c with Simpson's rule.

In addition, Table III tabulates the data used for Figure 7 and includes a column showing $\bar{G}_x$ calculated using two terms of the Taylor series. Except within the 0.2 semichord near the tip, all of the means of calculating the correction factor are in good agreement. The three-term approximation is in good agreement with the numerical integration calculation even closer to the tip.

As would be expected, the correction factor decreases rapidly as the distance from the tip is increased. The correction factor $\bar{G}_x$ is the change in velocity (ΔU_∞) between the two-dimensional and the three-dimensional flows. At the tip, for a 10% thick airfoil, $\Delta U_\infty/U_\infty$ is about 3.0%, while one semichord inboard it is reduced to 0.15%.

The magnitude of $\Delta U_\infty/U_\infty$ is indicative of the accuracy required in calculating $\bar{G}_x$. Since $\Delta U_\infty/U_\infty$ is of the order of one percent, a ten-percent error in $\bar{G}_x$ results in only a one-tenth of one percent error in U_∞.

The effect of aspect ratio on the correction factor may be noted in Figure 7. Here the aspect ratio effect is seen on the magnitude of the distribution of $\bar{G}_x$, especially at the wing center line, where differences in $\bar{G}_x$ for the various aspect ratios are seen to be important for the small aspect ratios considered.

Figure 8 compares the spanwise variation of the correction factor near the tip for several aspect ratios. It is seen that the differences are rather small. The difference between the aspect ratio 20 and the semi-infinite wing could not be shown on the plot as it is a difference of one in the third significant place. The effect of aspect ratio on the value of the correction factor near the tip is thus small, as any effect is due to the complementary wing associated with the opposite tip, and since it is far away, it has only a small effect.

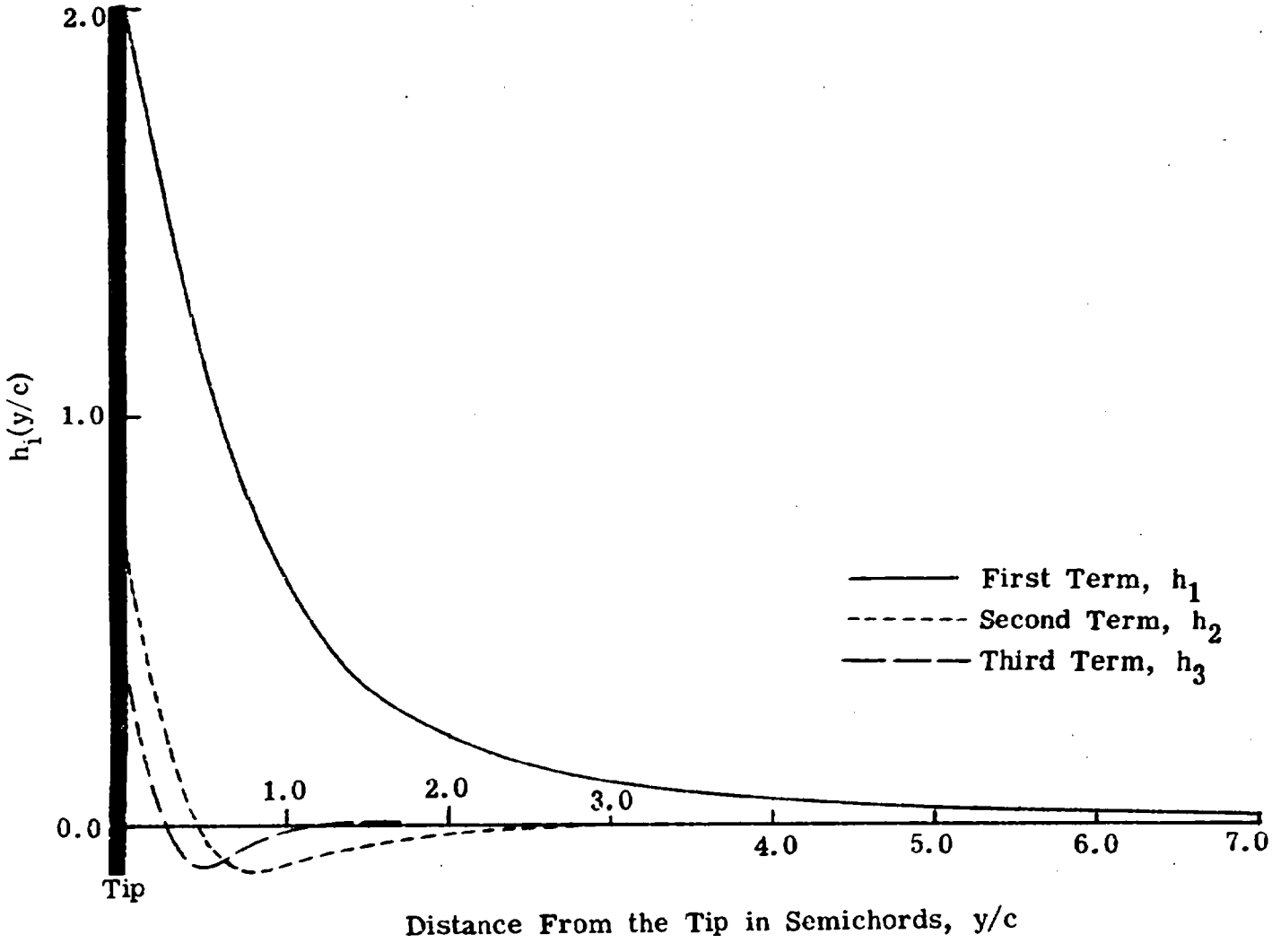

Figure 4. Coefficients of the Taylor Series for a Semi-Infinite Wing.

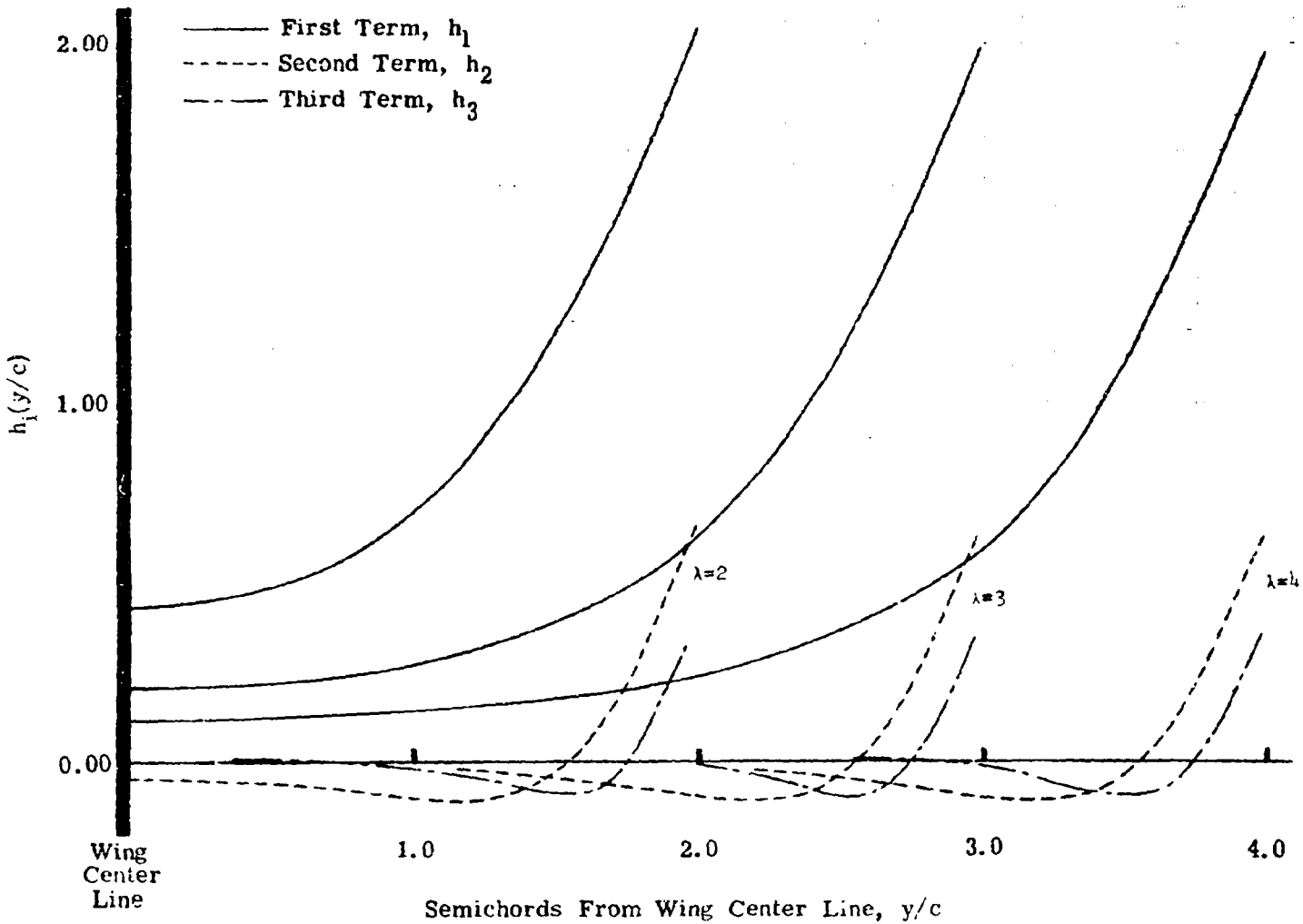

Figure 5. Coefficients of the Taylor Series for Finite Wings of Three Aspect Ratios With a 10% Thick Parabolic Arc Airfoil Section.

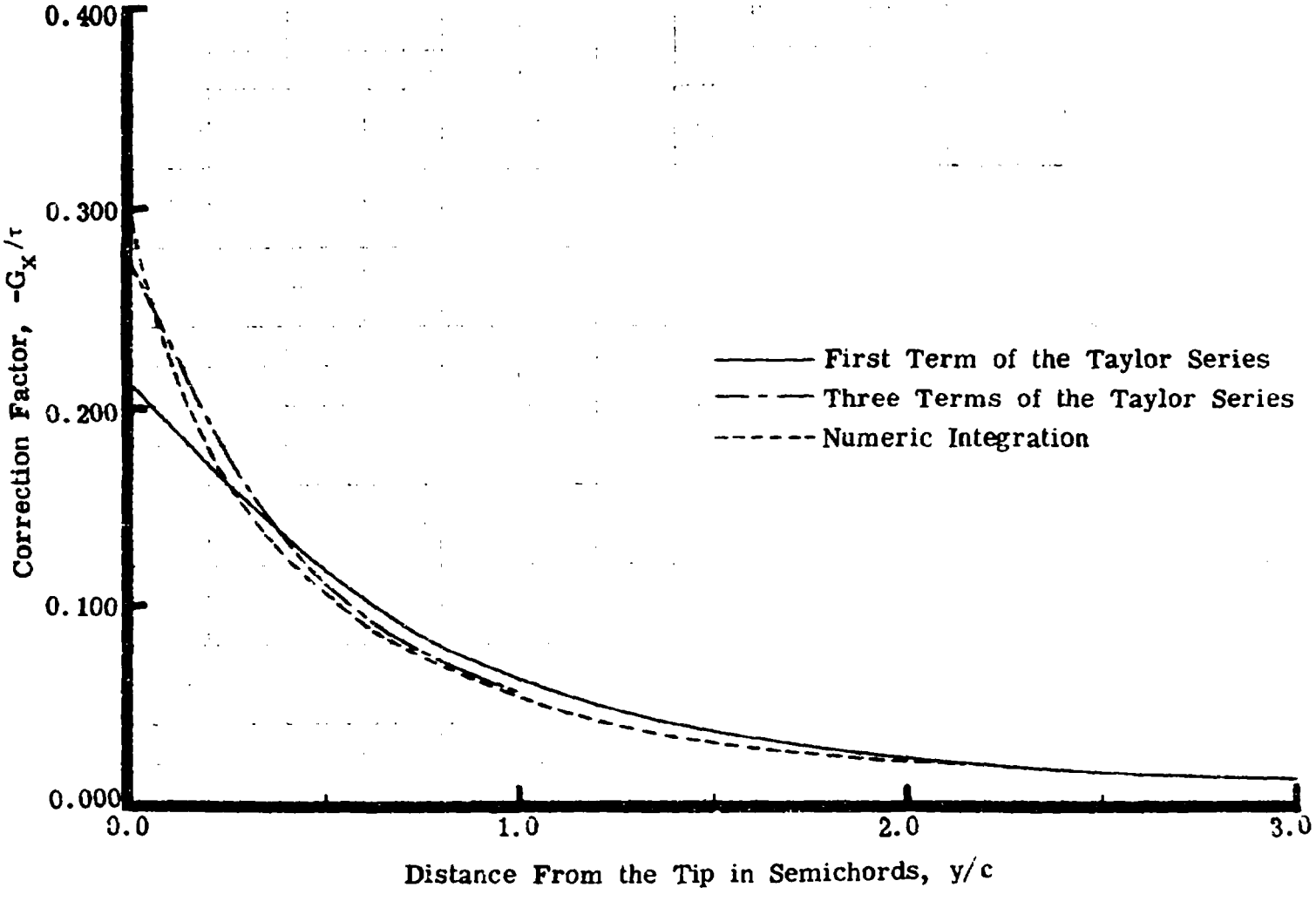

Figure 6. Correction Factor for a Semi-Infinite Wing With a Parabolic Arc Airfoil Section; Thickness = 10%.

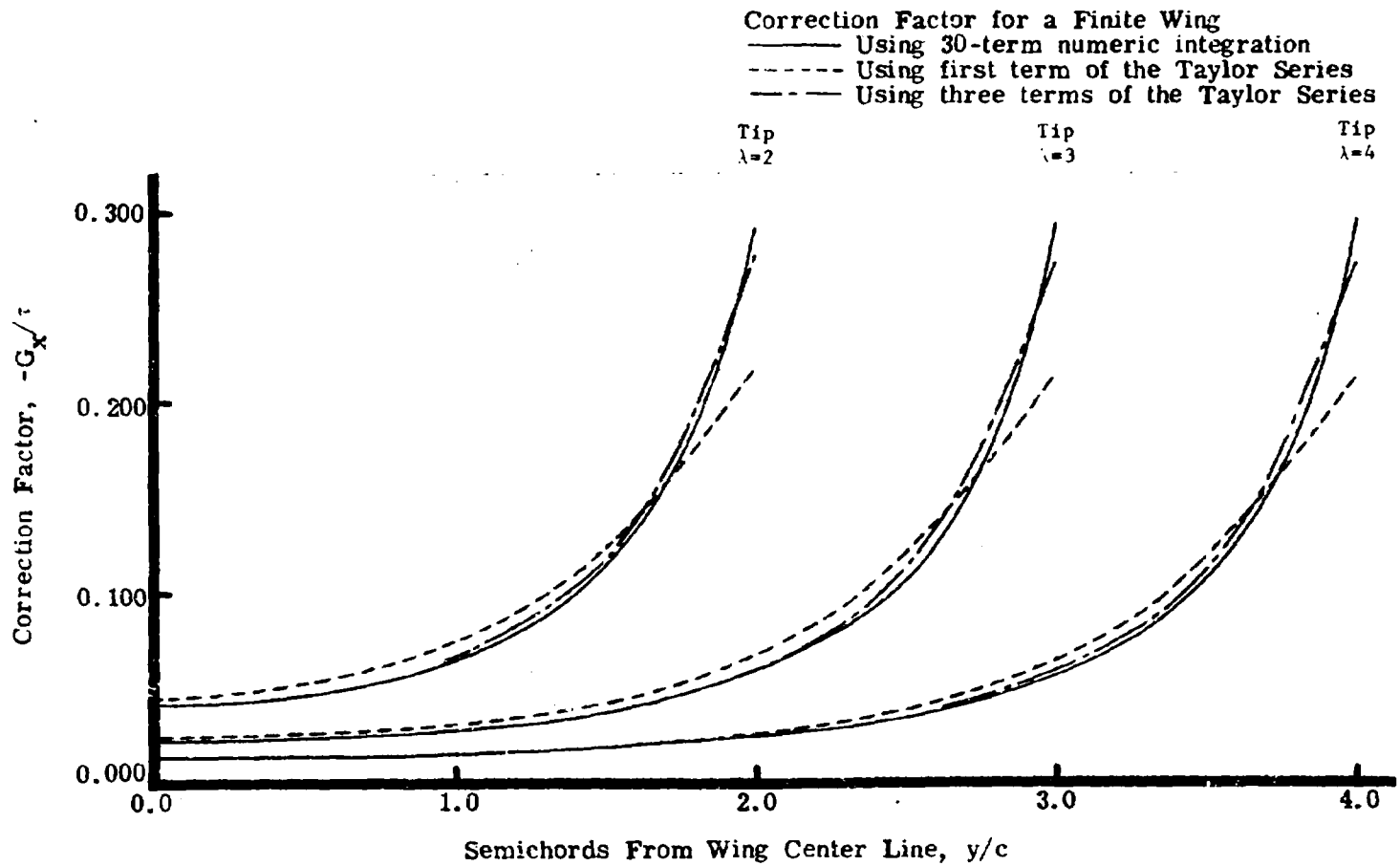

Figure 7. Correction Factor for Finite Wings of Three Aspcet Ratios With a 10% Thick Parabolic Arc Airfoil Section.

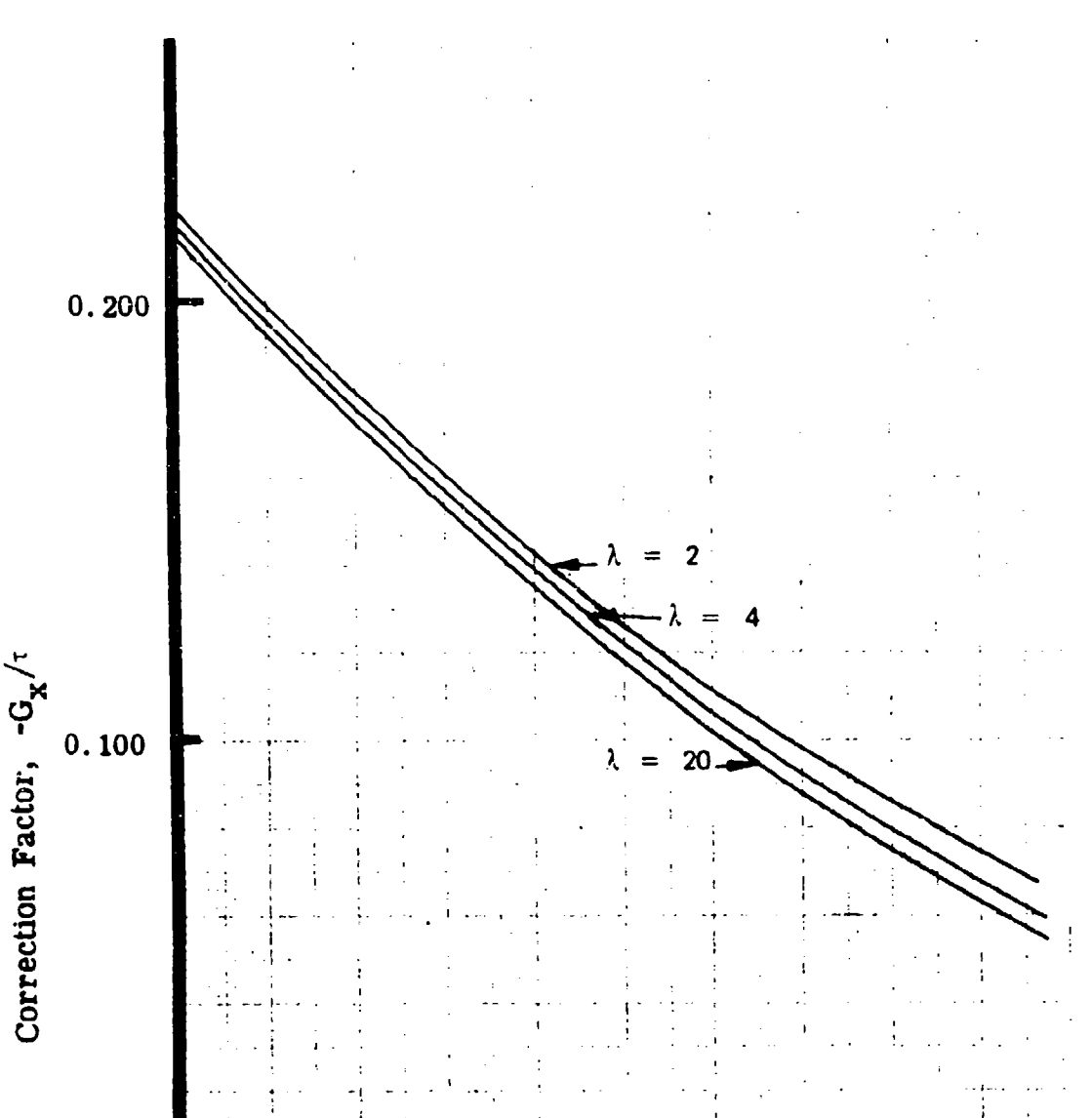

Figure 8. Effect of Aspect Ratio on the Correction Factor Calculated by the First Term of the Taylor Series.

TABLE III. CORRECTION FACTOR FOR A SEMI-INFINITE WING

SPAN	TERMS OF THE TAYLOR SERIES			INTEGRATED USING 30 TERMS
	FIRST	SECOND	THIRD	
0,00500000	-0,02111457	+0,02529505	+0,02706850	-0,02934514
0,01000000	-0,02100848	+0,02512531	+0,02685331	-0,02870782
0,01500000	-0,02090240	+0,02495562	+0,02663823	-0,02810082
0,02000000	-0,02079635	+0,02478600	+0,02642328	-0,02770379
0,02500000	-0,02069033	+0,02461648	+0,02620853	-0,02725842
0,05000000	-0,02016097	+0,02377112	+0,02513926	-0,02531807
0,10000000	+0,01910914	+0,02210093	+0,02304137	-0,02226477
0,15000000	+0,01807279	+0,02047623	+0,02103217	-0,01986488
0,20000000	-0,01705896	-0,01891626	+0,01914564	-0,01788802
0,25000000	+0,01607391	+0,01743656	+0,01742549	-0,01621630
0,30000000	+0,01512296	+0,01604843	+0,01582454	-0,01477810
0,35000000	+0,01421042	+0,01475888	+0,01442564	-0,01352551
0,40000000	+0,01333952	+0,01357091	+0,01314358	-0,01242437
0,45000000	+0,01251246	+0,01248410	+0,01202747	-0,01144918
0,50000000	+0,01173050	+0,01149527	+0,01104306	-0,01058252
0,55000000	+0,01099403	+0,01059927	+0,01017477	-0,00980226
0,60000000	-0,01030273	+0,00978962	+0,00940718	-0,00910248
0,65000000	+0,00965566	+0,00905918	+0,00872597	-0,00847270
0,70000000	+0,00905142	+0,00840055	+0,00811846	-0,00789841
0,75000000	+0,00848827	+0,00780649	+0,00757376	-0,00737844
0,80000000	+0,00796423	+0,00727012	+0,00708272	-0,00690471
0,90000000	+0,00702479	+0,00634590	+0,00623272	-0,00607594
1,00000000	+0,00621539	+0,00558281	+0,00552272	-0,00537851
1,09999999	+0,00551865	+0,00494740	+0,00492161	-0,00478781
1,20000000	+0,00491850	+0,00441262	+0,00440762	-0,00428185
1,29999999	+0,00440066	+0,00395817	+0,00396480	-0,00384770
1,39999999	+0,00395270	+0,00356860	+0,00358102	-0,00347242
1,50000000	+0,00356401	+0,00323203	+0,00324672	-0,00314629
1,75000001	+0,00279597	+0,00256672	+0,00258019	-0,00249802
1,99999999	+0,00224033	+0,00208102	+0,00209084	-0,00202332
2,25000000	+0,00182898	+0,00171663	+0,00172329	-0,00166724
2,50000000	+0,00151777	+0,00143711	+0,00144155	-0,00139445
2,74999999	+0,00127762	+0,00121863	+0,00122159	-0,00118155
3,00000001	+0,00108898	+0,00104506	+0,00104705	-0,00101263
3,50000001	+0,00081649	+0,00079092	+0,00079187	-0,00076573
3,99999999	+0,00063360	+0,00061784	+0,00061832	-0,00059784
4,49999999	+0,00050533	+0,00049515	+0,00049540	-0,00047895
5,00000000	+0,00041209	+0,00040524	+0,00040539	-0,00039190
6,00000001	+0,00028873	+0,00028532	+0,00028537	-0,00027585
7,99999997	+0,00016387	+0,00016275	+0,00016276	-0,00015732
10,00000000	+0,00010531	+0,00010485	+0,00010485	-0,00010134
19,99999998	+0,00002648	+0,00002645	+0,00002645	-0,00002556
50,00000000	+0,00000424	+0,00000424	+0,00000424	-0,00000410

Airfoil Section: Parabolic Arc
Thickness: 10%

Thus a result to be found later may be anticipated. In a rotor, which is a blade of large (on the order of 15 to 20) aspect ratio, a large part of the forces are near the tip, and this is where most of the correction needs to be applied. But near the tip, the actual aspect ratio has a second-order effect. Therefore, for rotary-wing calculations, the simplified semi-infinite wing correction factor will be found satisfactory.

CORRECTION FACTOR FOR A ROTATING WING

Sears,[12] in 1950, derived the relationship between the incompressible velocities on a rotating blade and on a similar cylinder in plane steady flow. The relation of the potentials is

$$\phi = \Omega y(\phi_1 - x) \tag{37}$$

where ϕ is the potential of the rotating blade and ϕ_1 is the potential of the blade in uniform flow at unit velocity.

The velocities in the transverse (to the span) plane are identical in the two cases. The spanwise component of the velocity is given by a very simple formula, and for an infinite circular cylinder this velocity is zero on the surface and therefore makes no contribution to the forces.

A recent paper extending Sears by Goorjian and McCroskey[13] indicates that for finite span rotating blades, there is a finite spanwise potential velocity at the surface. While this component is important in boundary layer calculations and thus affects the separation line, its contribution to the pressure in the linearized case being applied here is of the same order of magnitude as other terms which are neglected.

Therefore, for a rotating blade, we may write, from equation (37) and the discussion for fixed wings,

$$u = -\Omega y + \int_{\text{planform}} \frac{\Omega y}{2\pi} F_\xi \frac{(x-\xi)dS}{D^3} \tag{38}$$

where

$$D^2 = (x-\xi)^2 + (y-\eta)^2 + z^2 \tag{39}$$

and

$$dS = d\xi d\eta \tag{40}$$

In a manner similar to that used for the fixed-wing case, the integration over the finite planform may be split up as integration over the infinite blade less the integral over the complementary blade. Averaging over the chord results in

$$u = \Omega y \left[1 + \int_{-c}^{+c} \int_{-c}^{+c} \int_{tip}^{\infty} \frac{F_\xi}{4\pi c} \frac{(x-\xi)\,d\xi\,d\eta\,dx}{D^3} \right] + u_{\lambda = \infty} \qquad (41)$$

where $u_{\lambda = \infty}$ is the velocicy due to the infinite blade. The spanwise coordinate y in equation (38) may be brought outside of the integral sign since it is invariant with respect to each of the three variables of integrations. This equation is identical to the result obtained for the semi-infinite wing (equation (6b) with the averaging given by equation (9) and the integrand in equation (11)). Thus it has been shown that the correction factor in the case of a rotating blade is given by the same equation as for a fixed wing.

CORRECTION FO THE CHANGE IN DYNAMIC PRESSURE

The correction factor is the difference between the velocities of a finite wing and an infinite wing* having the same potential. This in turn means that the two wings have the same static-to-total-pressure ratio and therefore the same force acting,

$$D_{\text{finite wing}} = D_{\text{infinite wing}} \qquad (42)$$

with the velocity condition of equation (7), which requires different dynamic pressures. Thus, since the reference areas are also the same,

$$(C_D q)_{FW} = (C_D q)_{\lambda = \infty} \qquad (43)$$

but neither C_D nor q is the same. Thus

$$C_{D_{FW}} = C_{D_{\lambda = \infty}} \Big/ \left(1 + \frac{\Delta q}{q}\right) \qquad (44)$$

or by logarithmic differentiation of (43)

$$\Delta C_D / C_D = - \Delta q / q \qquad (45)$$

The correction gives the change in velocity and thus the change in dynamic pressure. Since the drag is a function of Mach number, the change in velocity must be applied not only as a change in drag coefficient but also as a change in Mach number as will be shown in Figure 10. It is more convenient to express both of these changes in terms of the free-stream Mach number.

In the introduction, the explanation of the tip relief effect was made on the basis of deviation allowed of the stream. Consider a representative stream tube as it passes over a finite and an infinite wing illustrated in

* While the discussion here talks about wings, since the correction factor was derived as it varies along the span of a finite wing, the discussion presented here is just as valid for a spanwise element of the wing located a given distance y from the tip.

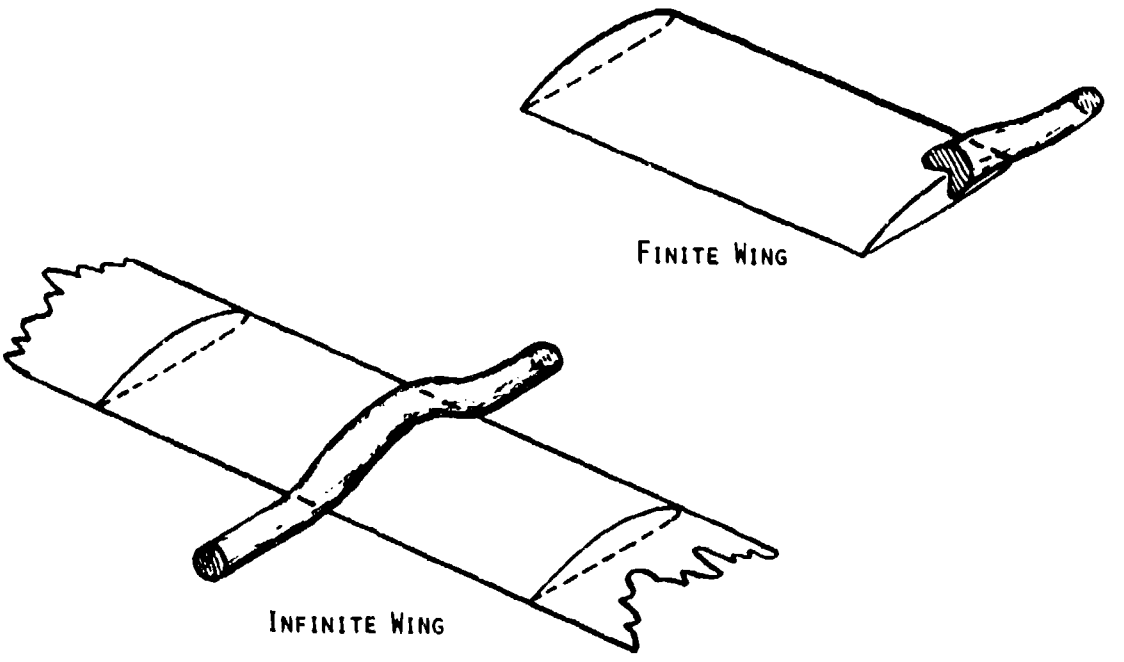

Figure 9. Distortion of a Stream Tube Over a Finite and an Infinite Wing.

Figure 9. In the case of the infinite wing, the stream tube cross-sectional area is decreased and displaced due to the displacement effect of the wing. But for the finite wing, the stream tube may also expand laterally; thus the cross-sectional area is decreased by a lesser amount.

The flow in both of these stream tubes is isentropic, and thus the usual quasi-one-dimensional isentropic, compressible flow analysis may be used. Since both stream tubes have identical conditions at infinity, they may be considered as part of the same stream tube. In the usual application of this analysis, the area changes are known. In this case, however, the velocity changes are given by the correction factor, while the area change in quantitative terms is immaterial. It is desired to find $\Delta C_D/C_D$ and $\Delta M/M$ in terms of $\Delta U/U \equiv -\bar{G}_x$, with the appropriate compressible transformation.

The equation of continuity for a stream tube may be written as either

$$\rho U A = \text{Const} \tag{46}$$

or

$$A\theta = \frac{\rho UA}{\rho^* U^*} = \frac{\rho_0}{\rho^*} \frac{\rho}{\rho_0} M^* A \tag{47}$$

where A is the area and the starred quantities represent conditions at a sonic point as a reference. Also Bernoulli's equation is

$$UdU + dp/\rho = 0 \tag{48}$$

Logarithmic differentiation of equation (46)

$$\frac{\partial \rho}{\rho} + \frac{\partial U}{U} + \frac{\partial A}{A} = 0 \tag{49}$$

combined with Bernoulli's equation leads to the familiar

$$(M^2 - 1)\frac{dU}{U} = \frac{dA}{A} \tag{50}$$

used so often in describing the difference between subsonic and supersonic flow. Using the relations from isentropic flow

$$\frac{\rho^*}{\rho_0} = \left(\frac{2}{\gamma - 1}\right)^{1/\gamma - 1} \tag{51}$$

$$\frac{\rho}{\rho_0} = \left(\frac{2}{(\gamma - 1)M^2 + 2}\right)^{1/\gamma - 1} \tag{51b}$$

$$M^{*2} = \frac{(\gamma - 1)M^2}{(\gamma - 1)M^2 + 2} \tag{51c}$$

Equation (47) results in, after some manipulation,

$$AM \left(\frac{\gamma + 1}{(\gamma - 1)M^2 + 2}\right)^{\frac{\gamma + 1}{2(\gamma - 1)}} = \text{constant} \tag{52}$$

Logarithmic differentiation gives

$$\frac{dA}{A} = \frac{2(M^2 - 1)}{((\gamma - 1)M^2 + 2)} \frac{dM}{M} \tag{53}$$

Combine equations (49) and (53):

$$\frac{dM}{M} = \left(1 + \frac{\gamma - 1}{2} M^2\right) \frac{dU}{U} \tag{54}$$

which is the relation between the velocity change as given by the correction factor and the resulting Mach number change.

Since $q = \rho U^2/2$, logarithmic differentiation gives

$$\frac{dq}{q} = \frac{d\rho}{\rho} + 2\frac{dU}{U} \tag{55}$$

Combining with equation (49) gives

$$\frac{dq}{q} = -\frac{dA}{A} - \frac{dU}{U} + 2\frac{dU}{U} = \frac{dU}{U} - \frac{dA}{A} \tag{56}$$

Substituting from equation (50) and then from equations (54) and (45),

$$\frac{dq}{q} = \frac{dU}{U} - (M^2 - 1)\frac{dU}{U} = (2 - M^2)\frac{dU}{U} \tag{57}$$

$$\frac{dC_D}{C_D} = -\frac{dq}{q} = -\frac{2 - M^2}{1 + \frac{\gamma - 1}{2} M^2} \frac{dM}{M} \tag{58}$$

As previously noted, the derivation here is applicable to a segment of a wing or to a full wing, depending on how the correction factor is derived. In fact, equations (54) and (58) are given by Anderson.[1] But since he did not give their derivation in detail or explain them in a physical manner, and since they are unusual in form, it is felt that presenting their derivation in detail would be useful in clearing up some misunderstandings.

Figure 10 illustrates the application of equations (54) and (58). The correction factor used here was from Reference 1 and for aspect ratio 3 wing with NACA 0012 airfoil with two-dimensional drag vs. Mach number characteristics approximated by two straight lines as proposed in Reference 55. A point on the two-dimensional curve is displaced horizontally in accordance with equation (54) and then vertically as per equation (58) to obtain the three-dimensional characteristic.

In reading this plot, the drag of the three-dimensional wing is seen to be less than the drag of the corresponding two-dimensional wing at the same Mach number.

Experimental verification of the basic theory for fixed wings may be found in the report by Anderson and Carroll.[43] Wings of various aspect ratios at high subsonic speeds are correlated both for the case of nonlifting wing and for the lifting case with lift coefficients up to 0.3.

The corrected drag coefficient as calculated for Figure 10, requires the use of appropriate transformation between the incompressible theory as derived here and the compressible flow considered. For this fixed wing case the direct Prandtl-Glauert transformation is used. For rotary wing, the extension discussed in the next chapter must be made to apply the transformation shown in equations (105) to (110).

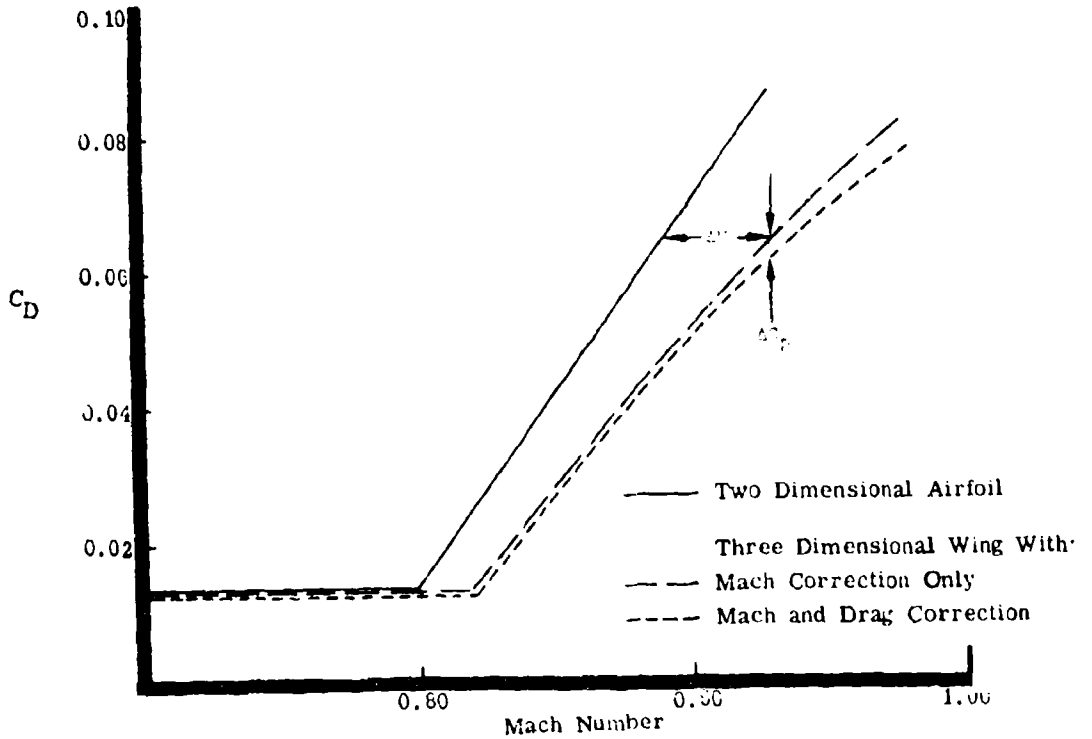

Figure 10. Theoretical Correction of the Drag Coefficient vs. Mach Number for an NACA 0012 Airfoil From Two-Dimensional Data to an Aspect Ratio of 3. (Note Displaced Origin.)

BASIC EQUATIONS OF A ROTOR IN COMPRESSIBLE FLOW

Having derived a tip relief correction for a fixed wing, the next step is the problem of applying this correction to a helicopter rotor. To do this, the basic fluid mechanic equations of a rotor have to be examined. Therefore, in this section the Navier-Stokes equations for a rotor in compressible flow will be written.

The usual approach to compressible flows is the small perturbation theory, and this derivation will be presented. In fixed-wing usage, the result is the Prandtl-Glauert transformation. It will be shown here that further assumptions are needed so that a Prandtl-Glauert type transformation between compressible and incompressible flows may be made for a rotor.

Previous work on the representation of a rotor in compressible flow by a system of sources and sinks was done by Sopher.[3] This work will be thoroughly reviewed to show how it is connected to the present presentation. The similarities and differences will be discussed, along with where each approach is useful.

FLUID DYNAMIC EQUATIONS FOR A ROTOR

Consider a coordinate system with a fixed origin O rotating with angular velocity Ω. The absolute velocity is $\vec{V}$, while the velocity relative to the rotating frame is $\vec{V}'$.* The relation between the two velocities is

$$\vec{V} = \vec{V}' + \vec{\Omega} \times \vec{r} \tag{59}$$

The equations relative to the rotating frame are the same as for a fixed frame except for the acceleration term

$$\frac{\partial \vec{V}}{\partial t} + \vec{V}' \cdot \nabla \vec{V} + \Omega \times \vec{V} \tag{60}$$

With some vector identities, we have

$$(\vec{V}' \cdot \nabla)\, \vec{V} = (\vec{V}' \cdot \nabla)\, \vec{V}' + \vec{\Omega} \times \vec{V}' \tag{61a}$$

$$\frac{\partial \vec{V}}{\partial t} = \frac{\partial \vec{V}'}{\partial t} \tag{61b}$$

$$\frac{\partial}{\partial r} (\vec{\Omega} \times \vec{r}) = 0 \tag{61c}$$

* This discussion is taken, to a large extent, from Hughes and Gaylord.[44]

Therefore, the equation of momentum is

$$\frac{\partial \vec{V}'}{\partial t} + (\vec{V}\cdot\nabla)\vec{V}' + 2\vec{\Omega} \times \vec{V}' + \vec{\Omega} \times (\vec{\Omega} \times \vec{r}) = -\nabla p \qquad (62)$$

where the last two terms on the left-hand side are due to the Coriolis and the centrifugal forces. Let the velocity $\vec{V}'$ have components v_r, $v_{\theta t}$, v_z in a cylindrical reference frame, and define the axis such that rotation is only about the z-axis. Further assuming, for convenience, steady flow with rotating coordinates, the three components of the momentum equation are

$$v_r \frac{\partial v_r}{\partial r} + \frac{v_{\theta t}}{r}\frac{\partial v_r}{\partial \theta} + v_z \frac{\partial v_r}{\partial z} - \frac{v_{\theta t}^2}{r} - 2v_\theta \Omega - r\Omega^2 = -\frac{1}{\rho}\frac{\partial p}{\partial r} \qquad (63a)$$

$$v_r \frac{\partial v_{\theta t}}{\partial r} + \frac{v_{\theta t}}{r}\frac{\partial v_{\theta t}}{\partial \theta} + v_z \frac{\partial v_r}{\partial z} + \frac{v_\theta v_r}{r} + 2v_r\Omega = -\frac{1}{\rho r}\frac{\partial p}{\partial \theta} \qquad (63b)$$

$$v_r \frac{\partial v_z}{\partial r} + \frac{v_{\theta t}}{r}\frac{\partial v_z}{\partial \theta} + v_z \frac{\partial v_z}{\partial z} = -\frac{1}{\rho}\frac{\partial p}{\partial z} \qquad (63c)$$

The equation of continuity is identical in rotating and stationary frames of reference:

$$\frac{\partial v_r}{\partial r} + \frac{1}{r}\frac{\partial v_{\theta t}}{\partial \theta} + \frac{\partial v_z}{\partial z} + \frac{v_r}{r} + \frac{v_r}{\rho}\frac{\partial \rho}{\partial r} + \frac{v_{\theta t}}{\rho r}\frac{\partial \rho}{\partial \theta} + \frac{v_z}{\rho}\frac{\partial \rho}{\partial z} = 0 \qquad (64)$$

Further, the speed-of-sound relation is

$$(\partial p/\partial \rho)_s = a^2 \qquad (65)$$

To combine equations (63), (64) and (65) by multiplying each of the equations in (63) by v_r, $v_{\theta t}$ and v_z, and by using equations (64) and (65) to put the pressure and the density in terms of the speed of sound gives

$$(v_r^2 - a^2)\frac{\partial v_r}{\partial r} + (v_{\theta t}^2 - a^2)\frac{1}{r}\frac{\partial v_{\theta t}}{\partial \theta} + (v_z^2 - a^2)\frac{\partial v_z}{\partial z} - \frac{v_r}{r}(2v_{\theta t} - a^2) - v_r r\Omega^2$$

$$+ v_{\theta t} v_r \left(\frac{1}{r}\frac{\partial v_r}{\partial \theta} + \frac{\partial v_{\theta t}}{\partial r}\right) + v_r v_z \left(\frac{\partial v_r}{\partial z} + \frac{\partial v_z}{\partial r}\right) + v_z v_{\theta t}\left(\frac{\partial v_{\theta t}}{\partial z} + \frac{1}{r}\frac{\partial v_z}{\partial \theta}\right) = 0 \qquad (66)$$

Because of the choice of axis, in terms of the its components $\vec{V}$ can be written as

$$\vec{V} = v_r \hat{e}_r + (v_\theta - \Omega r)\hat{e}_\theta + v_z \hat{e}_z \tag{67}$$

where $\hat{e}_r$, $\hat{e}_\theta$, $\hat{e}_z$ are unit vectors. The theta component is made up of two parts, one a "free stream" of magnitude $-\Omega r$ and a difference velocity v_θ, which together make up $v_{\theta t}$. The only rotational component in equation (9) is the Ωr component, thus we may write

$$(\nabla \times \vec{V})_r = \frac{1}{r}\frac{\partial v_z}{\partial \theta} - \frac{\partial v_\theta}{\partial z} = 0 \tag{68}$$

$$(\nabla \times \vec{V})_\theta = \frac{\partial v_r}{\partial z} - \frac{\partial v_z}{\partial r} = 0 \tag{69}$$

$$(\nabla \times \vec{V})_z = \frac{\partial v_z}{\partial r} + \frac{v_\theta}{r} - \frac{1}{r}\frac{\partial v_r}{\partial \theta} = -2\Omega \tag{70}$$

With these two conditions, equation (66) may be written as

$$(a^2 - v_r^2)\frac{\partial v_r}{\partial r} + (a^2 - (v_\theta + \Omega r)^2)\frac{\partial v_\theta}{\partial \theta} + (a^2 - v_z^2)\frac{\partial v_z}{\partial z} =$$

$$a^2 v_r/r - v_r v_\theta/r + 2v_r v_\theta \Omega + 4v_r \Omega^2 r + 2v_r (v_\theta + \Omega r)\frac{\partial v_\theta}{\partial r} + 2v_r v_z \frac{\partial v_r}{\partial z}$$

$$+ 2v_z (v_\theta + \Omega r)\frac{\partial v_\theta}{\partial z} \tag{71}$$

The energy equation

$$a^2 + ((\gamma - 1)/2)\,\vec{V} \cdot \vec{V} = \text{Constant} \tag{72}$$

may be used to relate the velocity components and the reference speed of sound a_∞ to the local speed of sound a. The reference speed of sound is the speed of sound in the undisturbed region of the fixed frame. In the rotating frame, this is the speed of sound at velocity $-\Omega r$; thus

$$a_\infty^2 + \frac{\gamma - 1}{2}(\Omega r)^2 = a^2 + \frac{\gamma - 1}{2}\vec{V}' \cdot \vec{V}'$$

$$= a^2 + \frac{\gamma - 1}{2}\left((-\Omega r + v_\theta)^2 + v_r^2 + v_z^2\right) \tag{73}$$

Therefore,

$$a^2 = a_\infty^2 - \frac{\gamma - 1}{2}\left(-2v_\theta \Omega r + v_\theta^2 + v_z^2\right) \tag{74}$$

If we also say that a velocity potential exists (due to equation (67)),

$$v_r = -\frac{\partial \phi}{\partial r} = -\phi_r \tag{75a}$$

$$v_\theta = -\frac{1}{r}\frac{\partial \phi}{\partial \theta} = -\phi_\theta / r \tag{75b}$$

$$v_z = -\frac{\partial \phi}{\partial z} = -\phi_z \tag{75c}$$

after some rearrangement, equation (71) becomes

$$\begin{aligned}
&\phi_{rr} + \{1 - (\Omega r/a_\infty)^2\}\,\phi_{\theta\theta}/r^2 + \phi_{zz} + \phi_r/r = \\
&\quad \phi_{rr}/a_\infty^2 \left\{-(\gamma-1)\phi_\theta \Omega + \frac{\gamma-1}{2}\left(\frac{\phi_\theta^2}{r} + \phi_z^2\right) + \frac{\gamma+1}{2}\phi_r^2\right\} \\
&\quad + \phi_{\theta\theta}/r a_\infty^2 \left\{-(\gamma+1)\phi_\theta \Omega + \frac{\gamma+1}{2}(\phi_\theta/r)^2 + \frac{\gamma-1}{2}\left(\phi_r^2 + \phi_z^2\right)\right\} \\
&\quad + \phi_{zz}/a_\infty^2 \left\{-(\gamma-1)\phi_\theta \Omega + \frac{\gamma-1}{2}\phi_r + (\phi_\theta/r)^2 + \frac{\gamma+1}{2}\phi_z\right\} \\
&\quad - \frac{(\phi_\theta/r)^2 \phi_r}{a_\infty^2 r} - \frac{2\phi_\theta\,\phi_r \Omega}{a_\infty^2 r} + \frac{2\phi_r}{a_\infty^2}\left(\frac{\phi_{\theta r}}{r} - \frac{\phi_\theta}{r^2}\right)\left(\frac{\phi_\theta}{r} - \Omega r\right) \\
&\quad + 2\frac{\phi_z \phi_r}{a_\infty^2}\,\phi_{rz} + 2\frac{\phi_r}{a_\infty^2}\,\frac{1}{r}\,\phi_{\theta z}\left(\frac{\phi_\theta}{r} - r\Omega\right)
\end{aligned} \tag{76}$$

It should be emphasized that this equation is still an exact equation. Its counterpart in uniform flow, for example, would be equation 32-17 of Heaslet and Lomax.[45] All terms on the right-hand side should vanish for the small perturbation equation. This is accomplished by assuming that the ratio of all of the velocity components to the speed of sound is much less than one. Further, it is assumed that gradients of the velocities are also small, so that cross products of velocities and velocity gradients are also small. Terms of the form

$$\Omega r \, v_i / a_\infty^2 \tag{77}$$

may also be neglected. The result is

$$\phi_{rr} + \phi_{zz} + (1 - (\Omega r/a_\infty)^2)\phi_{\theta\theta}/r^2 + \phi_r/r = 0 \tag{78}$$

In the case where $\Omega r/a_\infty$ is nearly one, the coefficient of the $\phi_{\theta\theta}$ term in the left-hand side of equation (76) becomes very small, and thus the term on the right-hand side must also be considered. It is obvious and analogous to the uniform flow case that the term of the form of equation (77) is the largest of the terms and we should write

$$\phi_{rr} + \phi_{zz} + (1 - (\Omega r/a_\infty)^2)\ \phi_{\theta\theta}/r^2 + \phi_r/r =$$

$$-\ (\gamma + 1)\ (\Omega/ra^2_\infty)\ \phi_\theta\ \phi_{\theta\theta} \tag{79}$$

For the pressure, we have

$$dp = -\rho d(\bar{V}\cdot\bar{V}/2) \tag{80}$$

Integrating between a point where $p = p_\infty$ and $V = -\Omega r$ and a point on the blade,

$$p - p_\infty = \frac{\rho_\infty + \rho'}{2}\ (\ (\Omega r)^2 - (\ (v_\theta - \Omega r)^2 + v_z^2 + v_r^2\ )\ )$$

$$= -\ (\rho' - \rho_\infty)(-\Omega r v_\theta + \frac{v_\theta^2 + v_z^2 + v_r^2}{2}\ ) \tag{81}$$

Again assuming that all velocities are small and that $\rho' << \rho_\infty$ results in

$$p - p_\infty = -\rho_\infty\ v_\theta\ \Omega r \tag{82a}$$

or, in terms of the pressure coefficient,

$$C_p = \frac{p - p_\infty}{\frac{1}{2}\rho_\infty (\Omega r)^2} = \frac{2v_\theta}{\Omega r} = \frac{2\phi_\theta / r}{\Omega r} \qquad (82b)$$

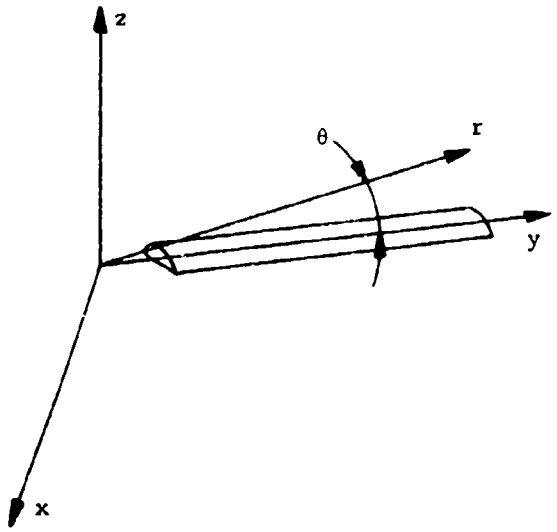

The basic equations (78) and (82) may be written in Cartesian coordinates, as suggested by Sears[12] and defined in Figure 11. Using the transformations

$$r^2 = x^2 + y^2$$

$$\theta = \tan^{-1}(-x/y)$$

$$x = -\, r \sin\theta \qquad (83)$$

$$y = +\, r \cos\theta$$

Figure 11. Coordinate System.

results in

$$\phi_{xx} + \phi_{yy} + \phi_{zz} = \frac{\Omega^2}{a^2_\infty} \left(-x\,\phi_x + y^2\phi_{xx} - 2\,xy\phi_{xy} - x^2\phi_{yy} - y\phi_y\right) \qquad (84)$$

$$C_p = \frac{2\,(y\phi_x - x\phi_y)}{\Omega(x^2 + y^2)} \qquad (85)$$

The results of equation (78) and (82) are identical to the results obtained by Sopher[3] directly from the acoustic equations. Similar work has been done for a rotating and advancing blade. Simonov and Christianovitch[46] derived the equivalent of equation (78) in a similar manner. Also, Burns[47] derived the equivalent of equation (84) directly. We have gone into details here so that the further approximations which need to be made may be better understood.

Using the transformation $\theta = \Omega t$ in equation (78) and (82) results in the acoustic equation

$$a_\infty^2 \nabla^2\phi = \phi_{tt} \tag{86a}$$

$$p - p_\infty = -\rho_\infty \phi_t \tag{86b}$$

DIRECT SOLUTION

Source in a Rotating Flow

Recently, Sopher[3] presented the solution of the small perturbation equations using a source-sink distribution approach. The potential due to a point source travelling on a rotational path is

$$\phi = -k/4\pi D \tag{87}$$

where k is the strength of the source and D the distance function referred to coordinates rotating with the blade, which is given in polar coordinates by

$$D^2 = rr'(\theta - \theta')^2 + (1 - \frac{\Omega^2 rr'}{a_\infty^2}) ((r - r')^2 + z^2) \tag{88}$$

where the primed coordinates refer to the location of the source and the unprimed coordinates are the field points where ϕ is to be evaluated. In deriving this distance function, higher order terms in the expansion for the cosine are neglected early in the derivation. A comparison with the more familiar distance function for uniform compressible flow in Cartesian coordinates,

$$D_{UF}^2 = (x - x')^2 + (1 - \frac{U_\infty^2}{a_\infty^2})\{(y-y')^2 + z^2\} \tag{89}$$

reveals certain similarities and differences. The form, of course, is very similar. But the compressibility term, namely, Mach number (U_∞/a_∞) in the uniform flow case, changes to the local Mach number at the root mean square radius

$$\bar{r} = \sqrt{rr'} \tag{90}$$

of the source and the field points. Further transformation to Cartesian coordinates of the first term results in a very complex expression.

The resemblance between the two equations may be made closer if it is assumed that the field points and the source points are close to each other. A further restriction is that the two points are near the y axis, which physically means narrow blades with the axis along the span of the blade.

There are several arguments as to why this should hold, the most important being that, if these points are far apart, D in equation (87) is large, making the contribution to ϕ very small. With this assumption, it can be said that the root mean square radius, $\bar{r}$, of equation (90) does not differ greatly from r or r'. This will also provide for the small-angle expansion of the transformations (see equation (83)), namely,

$$x = \bar{r} \sin\theta \approx \bar{r}\theta$$
$$y = -\bar{r} \cos\theta \approx -\bar{r} \tag{91}$$

With this, the approximation of the distance function for rotating flow in Cartesian coordinates is

$$D^2_{\substack{\text{Rot.}\\ \text{Approx.}}} = \bar{r}^2(\theta - \theta')^2 + \left[1 - \left(\frac{\Omega\bar{r}}{a_\infty}\right)^2\right]((r - r')^2 + z^2)$$
$$= (x - x')^2 + \left[1 - \left(\frac{\Omega y}{a_\infty}\right)^2\right]((y - y')^2 + z^2) \tag{92}$$

The resemblance between the distance functions in rotating and uniform flow is now much closer. The compressibility factor in rotating flow is not constant, and thus a "local Mach number" has to be defined:

$$M_y = \Omega\, y/a_\infty \tag{93}$$

which is the Mach number now used in blade element rotor analysis.

This derivation of the approximate distance function will be used as part of the justification of the approximations made here.

The potential of a rotor blade is the potential due to the sum of all the sources representing the blade. This is the surface integral over the planform area of the blade.

As was shown in equations (82), the pressure distribution and therefore the forces are related in compressible perturbation flow to the tangential velocity v_θ. Further, Sopher (unpublished notes for Reference 3) derived from the usual flow tangency condition that the required source distribution to describe the thickness of a rotating wing is

$$k\,(r', \theta', z = 0) = -2\,\Omega r\, F_\theta / r = -2\Omega\, F_\theta \tag{94}$$

where F defines the vertical z dimension of the blade. Equation (94) resembles the linearized uniform flow source distribution, namely, twice the free-stream velocity times the local slope. It is important to note that the slope required in equation (94) is the slope in the direction tangential to the rotation rather than normal to span.

The integral to be evaluated then becomes

$$v_\theta = \frac{1}{2\pi} \int_S \frac{\Omega r'(\theta-\theta')F_{\theta'}\,dS'}{D^3} \tag{95}$$

The surface of the integration is the planform area of the blade and in cylindrical coordinates $dS' = r'd\theta'dr'$. This integral was numerically integrated in Reference 3 with important refinements in the areas of using a uniformly valid surface flow speed and an equivalent linear theory tip Mach number.

The Complementary Wing Directly in Rotating Coordinates

An attempt to apply the reasoning of the previous section, the complementary wing approach in the case of a rotating blade represented by the source distribution in compressible flow, will now be made. Because of the variable dynamic pressure reference for the pressure coefficient, the total forces are related to the total local velocity, which is the sum of Ωr plus v_θ and will be denoted by V. Consider the integration required in equation (95); as previously, split the integration: from 0 to infinity minus from tip to infinity. Thus we can write the equation for total local velocity as

$$V = \Omega r + V_\theta = \Omega r - \frac{1}{2\pi}\int_c \int_0^\infty \Omega r' \,(\theta-\theta')\, F_{\theta'}\, r'\, d\theta'\, dr'/D^3$$

$$+ \frac{1}{2\pi}\int_c \int_R^\infty \Omega r'(\theta-\theta')\, F_{\theta'}\, r'd\theta'\, dr'/D^3 \tag{96}$$

where c represents the integration over the constant chord.

In the case of the fixed wing, Anderson[1] obtained a transformation between the finite wing and infinite wings. The transformation could be simplified because of the following two results:

(1) The complementary wing integral (i.e., the second integration in equation (96))reduces to a form such that it is a multiple of the free-stream term.

(2) The infinite span integral is a known function obtained from other theoretical work, from experiments, or from elsewhere.

The first criterion is easily met, as may be seen by inspection. The two terms, after the integral is carried out, will reduce to a form $\Omega(r + G)$ which may be used instead of Ωr. Thus, we may write

$$V = (\Omega r)_{\text{effective}} + V_{\theta\ \text{infinite blade}} \tag{97}$$

The problem occurs in relating the infinite span integral to a known function. In the fixed-wing problem this is the much-studied case of two-dimensional flow over an airfoil. Many two-dimensional, compressible flow airfoil data are available. Further, the Prandtl-Glauert transformation is available, so that the flow may be compared to incompressible flows. In this case, though, the flow over a rotor of infinite span in the compressible regime must be known, calculated, or measured in some manner. There appears to be no straightforward way of determining this value. Analytically, it brings problems such as supersonic flows, etc. Experimental testing is conceptually impossible.

The reason that this problem may not be approached in the direct manner is that there is a basic difference between fixed-wing and rotating-wing flows in the compressible regime. This was indicated by Sopher's results[3] as discussed previously.

In incompressible flow, Sears[12] showed that there was a straightforward relation between uniform flow and flow over the same body rotating. This same type of relation does not hold for the derivation shown above for compressible, rotating flow, to a large extent due to the fact that we do not yet have a transformation between compressible and incompressible flows. Therefore, how such a transformation might be obtained is described in the next section.

PRANDTL-GLAUERT TYPE TRANSFORMATION FOR A ROTATING BLADE

The basic differential equations in Cartesian coordinates (equations (84) and (85)) may be rewritten as

$$\phi_{xx} + \phi_{yy} + \phi_{zz} = \left(\frac{\Omega y}{a_\infty}\right)^2 \left(-\frac{x}{y^2}\phi_x + \phi_{xx} - 2\frac{x}{y}\phi_{xy} + \frac{x^2}{y^2}\phi_{yy} - \frac{1}{y}\phi_y\right) \tag{98}$$

$$C_p = \frac{2\left(\phi_x - \frac{x}{y}\phi_y\right)}{\Omega y\left(1 + x^2/y^2\right)} \tag{99}$$

Consider the differential equations at points far from the center of rotation. Now y is the spanwise distance and is of the order of magnitude of the radius. At the same time, x is of the order of magnitude of the chord. To compare the magnitude of each of the terms in the right-hand side of equation (98), nondimensionalize the x-dimension with the chord c and the y-dimension with radius R. (The primed coordinates in this section are nondimensional.)

$$\frac{\Omega^2 y'^2 R^2}{a^2_\infty}\left(-\frac{c}{R^2 c}\frac{x'}{y'^2}\phi_{x'} + \frac{1}{c^2}\phi_{x'x'} - 2\frac{x'c}{y'R}\frac{1}{Rc}\phi_{x'y'} + \frac{x'^2c^2}{y'^2R^2}\frac{1}{R^2}\phi_{y'y'} - \frac{1}{Ry'}\frac{1}{R}\phi_{y'}\right)$$

or

$$\frac{\Omega^2 y'^2 R^2}{a_\infty^2 c^2}\left[-\frac{c^2}{R^2}\left(\frac{x'}{y'}\phi_{x'}+2\phi_{x'y'}+\frac{1}{y'}\phi_{y'}\right)+\frac{c^4}{R^4}\frac{x'^2}{y'^2}\phi_{y'y'}+\phi_{x'x'}\right] \tag{100}$$

For helicopter rotor the ratio c/R is much smaller than one. The coefficients of all terms but one, (c/R), are raised to a power which will make all terms small in comparison with the term of order (1). Therefore, the differential equation becomes, when neglecting the higher order terms,

$$(1-(\Omega y/a_\infty)^2)\phi_{xx}+\phi_{yy}+\phi_{zz}=0 \tag{101}$$

In a similar manner, for the pressure coefficient,

$$C_p=\frac{2\left[\frac{1}{c}\phi_{x'}-\frac{c}{R}\frac{x'}{y'}\left[\frac{1}{R}\phi_{y'}\right]\right.}{\Omega y'\left(\frac{c^2}{R^2}\frac{x'^2}{y'^2}+1\right)} \tag{102}$$

As before, there are terms with a coefficient of one to compare with terms with coefficients $(c/R)^2$, which are small and neglected, so that

$$C_p=2\phi_x/\Omega y \tag{103}$$

Now equation (101) resembles very closely the Prandtl-Glauert equations of uniform flow, but with a variable Prandtl-Glauert factor

$$\beta^2_y=1-(\Omega y/a_\infty)^2=1-M_y^2 \tag{104}$$

This indicates that a Prandtl-Glauert type transformation may be made locally for a rotating blade. The usual illustration for the Prandtl-Glauert transformation is by the change in chord length (for example see Shapiro,[39] page 320). For a rotor, this change in chord length varies along the span due to the variable local Mach number. The resulting equivalent incompressible flow rotor is illustrated in Figure 12.

Since we now have a transformation between the compressible and the incompressible flows over a rotor, the complementary wing effect as derived in the previous section may be applied.

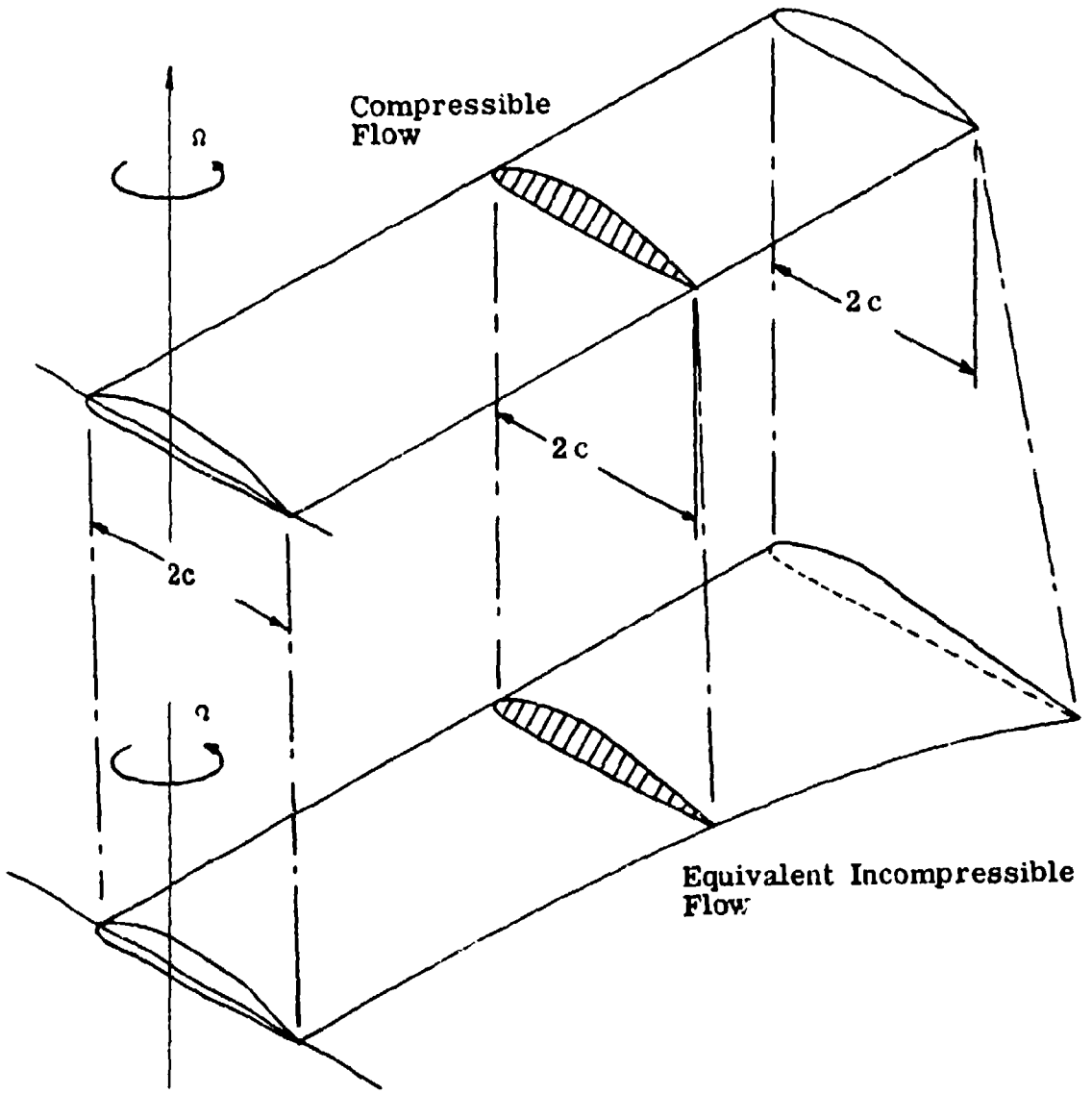

Figure 12. Prandtl-Glauert Type Transformation of a Rotor.

A short discussion of the implications of this approximation is in order. This approximation is consistent with blade element analysis, where an element of the blade is assumed to act as a similar airfoil in uniform two-dimensional flow. The transformation has been applied previously, without proof, for example, by Jones and Rao.[48]

The approximation is made of the initial equation used by Sopher.[3] Thus the differences found by Sopher between three-dimensional rotating flow theory and blade element analysis in the local induced velocities apply when using the proposed transformation. The problem with the analysis presented by Sopher is one of application. The major use of the Sopher analysis would be in boundary layer calculations where it is important to know the local velocity gradients, and where Sopher's analysis does give a previously unknown spanwise pressure gradient.

For the purposes of preliminary design and gross performance prediction, the approximations made here are consistent, and the Prandtl-Glauert type transformation may be safely used.

EXTENSIONS OF THE COMPRESSIBLE FLOW TRANSFORMATIONS

The Prandtl-Glauert transformation underpredicts the increase in flow speed with Mach number as may be seen in Figure C8a of Reference 49. Also, the Goethert extension to three-dimensional flows considers only the effect of compressibility on lift and the lift curve slope. This is done through the change in wing aspect ratio, since the Prandtl-Glauert transformation changes the chord but does not alter the spanwise or the thickness coordinates. No mention is made of any effect of compressibility on the three-dimensional drag.

There have been a number of attempts to obtain similarity rules that would extend the Prandtl-Glauert transformations to higher Mach numbers. The most important of these for two-dimensional flow were reviewed and compared by Bennett.[50] Van Dyke's second-order theory[51,52,52] is considered to give the best compressible pressure distributions of these techniques, but its use is rather complex. This method takes into account squares and products of the thickness, camber and angle-of-attack terms.

But a method suggested by Kuchemann and Weber[54] appears to be much simpler to apply. The usual form for the transformation is modified to the form

$$\beta^2 = 1 - M^2(1 - C_{pi})$$

where C_{pi} is the incompressible flow pressure distribution. This form was suggested for use in calculating local velocities and pressures as C_{pi} is a function of position.

A simple use of the latter transformation was suggested by Sopher[1] for rotors; namely, that an average value of C_{pi} be used, which can be considered constant along both the span and the chord. Thus for a rotor, $(\Omega r/a_\infty)\sqrt{1-C_{pi}}$ is an equivalent Mach number which may be used in the linear theory.

APPLICATION OF THE TIP RELIEF EFFECT IN ROTOR PERFORMANCE CALCULATIONS

Having derived a correction factor for the effective free stream to relate the two-dimensional airfoil data to three-dimensional wing characteristics, and a transformation between compressible and incompressible flow over a rotor, we are now ready to use this theory in helicopter performance calculations, which are based on blade element analysis.

Blade element analysis involves a long and complicated computer program. These programs are generally available to those who would use the theory, although it was not available for use within the present study. Therefore, the theory is not used in a full blade element analysis. Presented herein is a detailed description of how one should modify existing blade element computer programs to use the tip relief theory, and a simplified blade element analysis for a hovering rotor using the theory, so that an indication of the tip relief effect may be found.

THE PHYSICAL CONCEPT OF TIP RELIEF APPLIED TO A ROTOR BLADE ELEMENT ANALYSIS

The application of the tip relief concept to rotors in compressible flow requires that a physical model be postulated for the planform of the complementary wing. This planform is not immediately obvious as it is for the case of wings in uniform flows. In applying the complementary wing concept to calculate the effect of tip relief on rotors, full use is made of the blade element theory while extending it, and of the Prandtl-Glauert transformation with the extension to rotors as has been derived here.

Blade element analysis of rotors is based on the theory that an elemental spanwise segment of a rotor blade acts as a similar segment of a two-dimensional airfoil. The angle of attack (α), Mach number (M_y) and Reynolds number (Re) of the blade element are determined from the motion at the element including rotation, advance, flapping, etc., velocities and from the induced velocity. Since each element is considered independent of the adjoining elements, the force on the element is determined from the force coefficients of the similar two-dimensional airfoil at the angle of attack, Mach number, and Reynolds number calculated. The total thrust and torque of the rotor are obtained by integrating the contribution of each individual element along the blade span and the azimuth of the rotor disc.

Consider a straight, rectangular rotor blade of radius R and a constant chord c_o, rotating at an angular velocity Ω in compressible flow, as shown in Figure 13 (a). A specific element is located at a distance r from the center of rotation, i.e., a distance $y = R - r$ from the tip, and the element is at a local Mach number denoted by M_y.

The application of the Prandtl-Glauert type transformation to the rotor in compressible flow results in a nonuniform chord blade in the incompressible flow, as was illustrated in Figure 4. Now the complementary wing has to be applied and the question becomes that of postulating the planform of the complementary wing. Attempts to apply a nonuniform chord complementary wing led to physical and mathematical difficulties and thus was discarded. If instead, blade element theory is applied directly, then each element of the blade can be considered as part of an infinite span airfoil at the local velocity, Mach number, and local chord in uniform flow. The blade element theory may be extended, so that instead of an infinite span airfoil, the aerodynamics of the rotating element is characterized by an element located at the same spanwise distance from the tip of a finite wing, whose span is the same as that of the rotating blade. The complementary wing then is of constant chord to infinity and the results of the previous chapter may be applied. To summarize, an element at r of a blade rotating in compressible flow at a local Mach number M_y has the same tip relief effect as an element located at R - r of a similar wing of span R, with chord $c_o / \sqrt{1 - M_y^2}$. This is illustrated in Figures 13 (a) through (c).

This may also be approached by applying the blade element theory first and only then the Prandtl-Glauert transformation. Since both transformations are linear, their order is immaterial. Using the extended blade element theory, an element of the rotating blade has the same aerodynamic characteristics as an element at a distance y from the tip of a wing with span R, with constant chord c_o, travelling at a uniform velocity Ωr and Mach number M_y. To this wing is then the Prandtl-Glauert transformation applied, changing the constant chord to a new value $c_o / \sqrt{1 - M_y^2}$. The final result is physically and mathematically the same from either approach, although the latter may be more satisfying physically at the intermediate step.

In both approaches the assumptions made in deriving the Sears[12] relation between rotating and uniform flow are not thoroughly observed. In the first approach, a cylinder with a varying chord is transformed to plane flow; while in the second, the transformation is applied to compressible flows. These extensions of Sears' theoretical work are those that are used in all blade element analyses. In addition, the transformation is used for the finite span case.

Some theoretical validity for the blade element approach as extended to the use with finite span was recently given by Caradona and Isom.[56] They calculated the chordwise pressure distribution for a nonlifting rotor in compressible, inviscid flow and compared it to the pressure distribution on a wing at a similar spanwise position at the tip Mach number. The results show good agreement, except in areas affected by shocks.

An indication of the need for the use of finite rather than infinite aerodynamic characteristics in blade element theory may be found in this paper

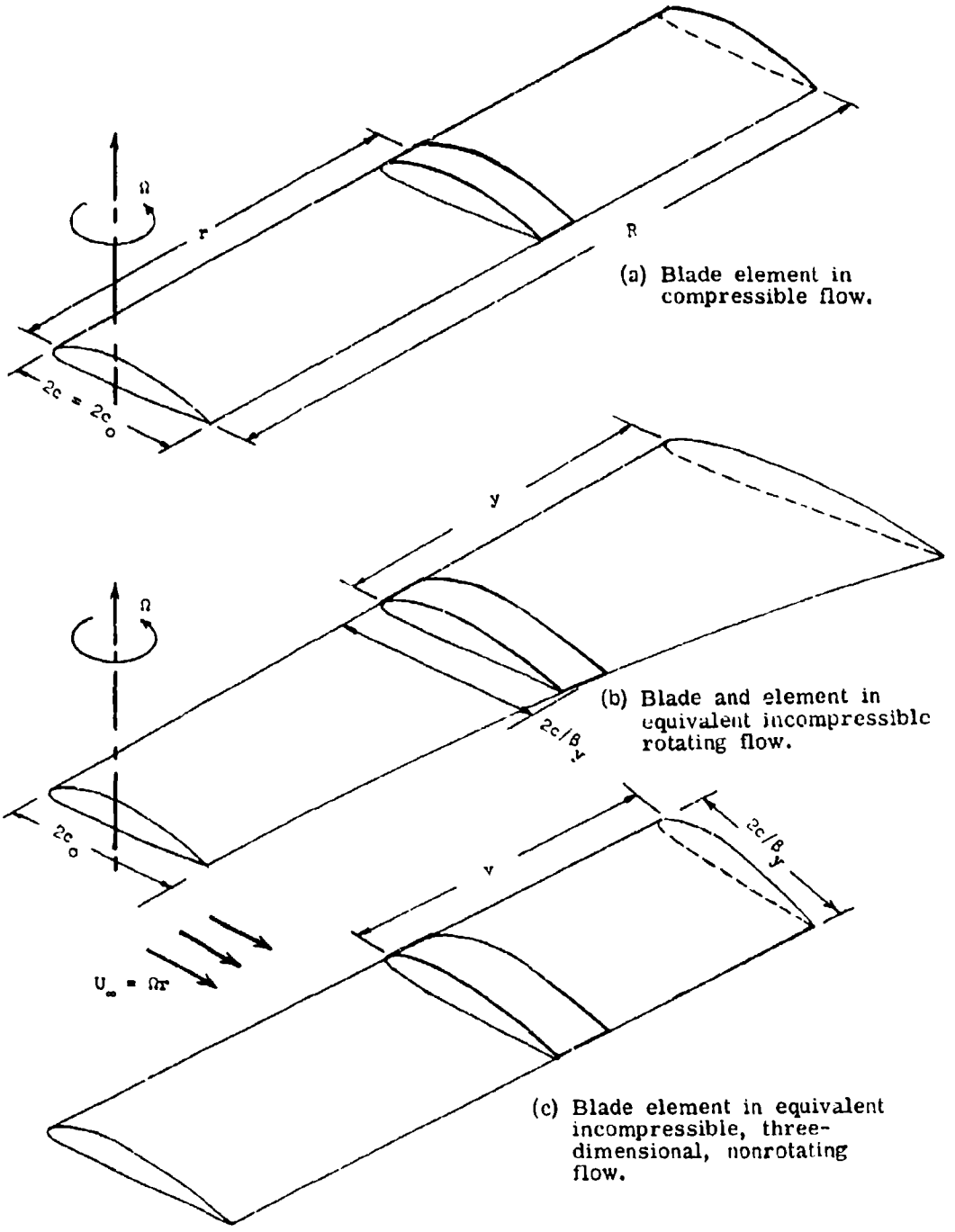

Figure 13. Transformation of a Rotor Blade Element.

by Caradona and Isom.[56] They compare the chordwise pressure distribution at similar spanwise stations on a rotor and on a wing at Mach number of the rotor tip. This differs from the blade element theory extended here, as a wing at a different Mach number is to be used at each station. For the first one-half semichord, there is no perceptible difference in their figure presenting this result.* Further inboard, the rotor has a lower (negative) pressure coefficient (i.e., smaller perturbation velocities) than the wing at the tip Mach number. This is also true at all stations when the Mach number is such as to cause local supersonic speeds. The result may be expected since the effective Mach number on the blade is lower than on the wing to which it is compared.

For compressible flow, we must further apply the local Prandtl-Glauert type transformation derived previously. As is usual in fixed-wing type flows, this correction is made to the chord:

$$c_c = c_i \beta_y \tag{105}$$

thickness ratio:

$$\beta_y \tau_c = t_i = t_i/c_i \tag{106}$$

aspect ratio:

$$\lambda_c = \lambda_i / \beta_y \tag{107}$$

perturbation velocity:

$$\Delta u_c = \Delta u_i/\beta_y^2 \tag{108}$$

The free-stream velocity does not change:

$$U_{\infty c} = U_{\infty i} \tag{109}$$

Therefore, the correction factor changes:

$$\overline{G}_{x_c} = \overline{G}_{xi}/\beta_y^2 = \Delta u_c/U_\infty \tag{110}$$

TIP RELIEF CALCULATION IN BLADE ELEMENT ANALYSIS

The tip relief effect is included quantitatively in blade element analysis by correcting the two-dimensional airfoil data in accordance with the theory presented here. The method for making this application in blade element computer programs will be described in a step-by-step manner.

*For $M_{tip} = 0.85$ the difference is less than 0.01 at this station.

1. In blade element analysis computer programs, the airfoil data, especially the drag coefficient, is available in some form as a function of angle of attack, Reynolds number, and Mach number.

2. At the blade element under consideration, the velocities are determined; thus angle of attack, Reynolds number, and Mach number can then be determined.

3. The correction factor for the blade element, knowing the distance of the element from the tip, is calculated using the method described before. Here, one can represent the wing as a semi-infinite or finite aspect ratio wing and use one or three terms of the Taylor series or a numerical integration scheme to obtain the correction factor.

4. Calculate $\beta_y^2 = 1 - (\Omega r/a_\infty)^2$ for the element and transform the correction factor to the compressible case (see equation (110)).

5. Find the effective Mach number (M_{eff}), using equation (54).

6. Obtain from the airfoil data the drag coefficient at the α and Re obtained in step 2 and at the M_{eff} obtained in step 5.

7. Calculate $\Delta C_D/C_D$, using equation (58).

8. Determine C_{Deff}, combining the drag coefficient found in step 6 and the drag correction $\Delta C_D/C_D$ found in step 7. Use this effective drag coefficient in calculation of the drag force of the element.

These steps are, of course, repeated for each segment each time as they are calculated during the iterations.

A SIMPLIFIED BLADE ELEMENT ANALYSIS

To obtain an indication of the magnitude and variation of the tip relief effect, a greatly simplified blade element analysis is derived for the case of a hovering rotor. These gross simplifications allow the use of a short computer program to make the integration over the rotor radius. The assumptions to be made will be discussed in turn as they are made.

The first assumption to be made concerns the form of the drag coefficient and its variation with Mach number. It is often (for example, Reference 55) approximated by the equations

$$C_D = C_{Di} \qquad 0<M<M_{crit}$$

$$C_D = C_{Di} + a_c (M - M_{crit}) \quad M_{crit}<M<1.0 \qquad (112)$$

or infinite aspect ratio. For an NACA 0012 airfoil section, most commonly used in rotor blades,

$$M_{crit} = 0.8$$

$$a_c = 0.57 \tag{113}$$

As previously noted, the correction for tip relief is made up of two parts: a change in the Mach number ΔM and a change in the drag coefficient ΔC_D, as obtained from equations (54) and (58) respectively. An inspection of Figure 9 will indicate that the change in Mach number is by far more important than the change in drag coefficient. Note that the change in Mach number assures a change in the drag coefficient in the subsonic drag rise range of Mach numbers. Therefore, in this simplified analysis the change in drag coefficient will be neglected.

From equation (112), the drag coefficient for a finite wing may be written as

$$C_{D_{FW}} = C_{D_i} + a_c \left((M - \Delta M) - M_{crit}\right) + \Delta C_D \tag{114a}$$

or rearranging slightly,

$$C_{D_{FW}} = C_{D_i} + a_c \left((M - M_{crit}) - M\right) + C_D \tag{114b}$$

Inspection of this equation indicates that the drag coefficient of a finite wing is made up of three parts:

1. The incompressible drag of an infinite wing $\sim C_{D_i}$
2. A correction for the compressible drag rise $\sim a_c (M - M_{crit})$
3. A correction for the tip relief effect made up of two terms $\sim -a_c \Delta M + \Delta C_D$

The ΔC_D term may be neglected for the reasons discussed above. It should be pointed out that by neglecting the ΔC_D term, the tip relief effect is assumed negligible below M_{crit}, since the drag coefficient is independent of Mach number as stated in the first of equation (112).

The torque of an element of a rotor blade due to drag is

$$dQ = rdD \cos\phi$$

$$= \rho (\Omega r)^2 \, 2c \, C_D \, r \, dr \, \frac{\cos\phi}{2} \tag{115}$$

The usual small-angle assumption is made. Since the equation (equations (114)) for the drag coefficient is linear, upon substituting into equation (115), the change in torque on the element due to tip relief may be separated and is

$$d\Delta Q = \rho(\Omega r)^2 \; 2c \; a_c \; \Delta M \; r dr/2 \tag{116}$$

or in coefficient form for b hovering rotor blades

$$d\Delta C_Q = \frac{1}{2} \frac{b2c}{\pi R} a_c \Delta M \; \bar{r}^3 d\bar{r} \tag{117}$$

From the definition of solidity and the transformation of equations (105) and (107),

$$\sigma_c = \frac{2bc_c}{\pi R} = \frac{2b}{\pi R} c_i \beta_y = \beta_y \sigma_i = \frac{b\beta_y}{\pi \lambda_i} \tag{118}$$

Using equations (54) and (118) in (117),

$$d\Delta C_Q = \frac{1}{2} \frac{\sigma_c}{\beta_y} a_c (1 + \frac{\gamma-1}{2} M^2) \; (\bar{G}_x/\beta_y^2) \; \bar{r}^3 \; d\bar{r} \tag{119}$$

Integrating,

$$\Delta C_Q = \frac{\sigma_i a_c}{2} \int_0^1 \frac{M}{\beta_y^3} (1 + \frac{\gamma-1}{2} \; M^2) \bar{G}_x \bar{r}^3 d\bar{r} \tag{120}$$

It should be emphasized that M, β_y and $\bar{G}_x$ are all functions of the radial position along the blade. Also note that $\bar{G}_x$ depends on F, the airfoil coordinates, whose thickness must be transformed in accordance with equation (106).

In equation (120) the correction factor needs to be calculated separately. In the simplest case, the correction factor is obtained by assuming a semi-infinite wing and using the first term of the Taylor series expansion. The change in Mach number then becomes, using equation (23b) (35c) and (54),

$$\Delta M/M = (1 + \frac{\gamma-1}{2} M^2) \; 2 \; (1 - \frac{1}{\sqrt{(c/y)^2 + 1}}) \; I_1/(4\pi\beta_y^2)$$

$$= 2(1 + \frac{\gamma-1}{2} \; M^2) \left[1 - \frac{1}{\sqrt{(1/(\beta_y \lambda_c (1-\bar{r})2)^2 + 1}}\right] \frac{I_1}{\tau} \frac{\beta_y \tau}{4\pi\beta_y^2} \tag{121}$$

The factor 2 occurs because 2λ=R. The value of I_1/τ is given in Table II. Substituting into equation (116) results in the integral

$$\Delta C_Q = \frac{\sigma \tau a_c}{4\pi} \left(\frac{I_1}{\tau}\right) \int_0^1 \frac{M r^{-3}}{\beta_y^2} \left(1 + \frac{\gamma-1}{2} M^2\right) \left[1 - \frac{1}{\sqrt{\left(\frac{1}{2\beta_y \lambda_c (1-\bar{r})}\right)^2 + 1}}\right] d\bar{r} \qquad (122)$$

Even in the simplest case of using the correction factor as for the first term of the Taylor series for a semi-infinite wing, as shown in equation (122), the integration of equation (120) appears to be too complicated to be analytically integrated. Therefore, three computer programs to numerically carry out the integration were written; they are listed in order of complexity:

1. A program using only the first term of the Taylor series for a semi-infinite wing only as the correction factor, as in equation (122).

2. A program using the Taylor series as the correction factor with options for using only the first or all three terms of the series and a finite or a semi-finite wing.

3. A program using the numerically integrated version of the correction factor.

These programs are similar and, therefore, will be described together. They use the trapezoidal rule for the integration, with a maximum of 50 steps and the values of the independent variable (rotor radius) given as input data. Each program consists of a main program, which sets up the necessary variables and contains the integration loop. To calculate the integrand, a function subroutine is called. The correction factor is calculated within the function in program 1; for the other two programs, the correction factor is calculated in a further subroutine.

In the third program, the correction factor is calculated by numerically integrating equation (16) as described on page 15. For parabolic arc airfoil shapes, 22 evenly divided segments were used along the chord from 0.0000 to 0.9999 (since this airfoil is symmetric about the $\xi = 0$ axis), while 30 points from +0.3999 to -0.9999 were used for the NACA 0012 airfoil.

Because of the assumptions made concerning the drag coefficient, there is no effect on the torque due to tip relief on any segment where the local Mach number is below eight-tenths. Also, there is a strong singularity at tip; therefore, the upper limit is 0.999950 rather than exactly one. Forty-nine unevenly spaced segments are used. Using only 39 segments in some test cases resulted in a change only in the third significant figure, but since there is only a small increase in computing time, 49 segments are used. The intervals were chosen so that the values of the integrals from the segments are roughly equal.

RESULTS

The computer programs discussed previously were run with a number of sets of data, with the various options available for calculating the correction factor. The results from these computer runs are discussed, as is the problem of comparison with experiment.

In making these calculations many major assumptions were made, the most important being the simplified form of the drag coefficient and neglecting the ΔC_D term in the tip relief correction on page 56. These assumptions are such that there is no variation of torque due to tip relief with lift. To make full use of the theory presented here, it should be applied to the drag coefficient used in a strip analysis computer program.

It should be noted in regard to the accuracy required that the calculation is of the change in torque coefficient due to tip relief. The order of magnitude of C_Q is about 25×10^{-5}, while at the same time the change in torque coefficient due to tip relief is about 2×10^{-5}. Thus, there is a factor of 10 between these two numbers, which are subtracted from each other. Three-place accuracy on ΔC_Q requires four-place accuracy of C_Q.

Results from the computer output indicate the differences between the various means of calculating the tip relief. This is summarized in Table IV. The choices are the use of finite and semi-infinite wing, and the use of numerical integration and one- and three-term Taylor series approximation. Further, calculations were made using parabolic arc and NACA four-digit series airfoil.

TABLE IV. CHANGE IN TORQUE DUE TO TIP RELIEF

Tip Mach Number, M	Solidity Per Blade	$-\Delta C_Q$ Per Blade	
		Finite Wing	Semi-Infinite Wing
	Using three terms of the Taylor series		
0.85	.0159	1.026×10^{-5}	1.024×10^{-5}
0.90	.0159	1.847	1.841
0.95	.0159	3.812	3.796
0.85	.0232	1.836	1.830
0.90	.0232	3.369	3.352
0.95	.0232	6.748	6.699
	Using numerical integration		
0.85	.0159	.993	.991
0.90	.0159	1.789	1.784
0.95	.0159	3.708	3.693
	Using the first term of the Taylor series		
0.85	.0232	1.718	1.711
0.90	.0232	3.180	3.162
0.95	.0232	6.203	6.153

Parabolic arc airfoil

The differences between the use of finite and semi-infinite wings for calculating ΔC_Q are very small. The differences are in the third significant figure, and thus it is recommended that calculations be made using the semi-infinite wing concept. Further discussion will be restricted to the semi-infinite case.

Figure 14 shows the change in torque coefficient due to tip relief obtained from the three means of calculating the correction factor. The numerical integration requires much more computing time, but since the differences are fairly small, it is believed that the use of the first term of the Taylor series will give satisfactory results.

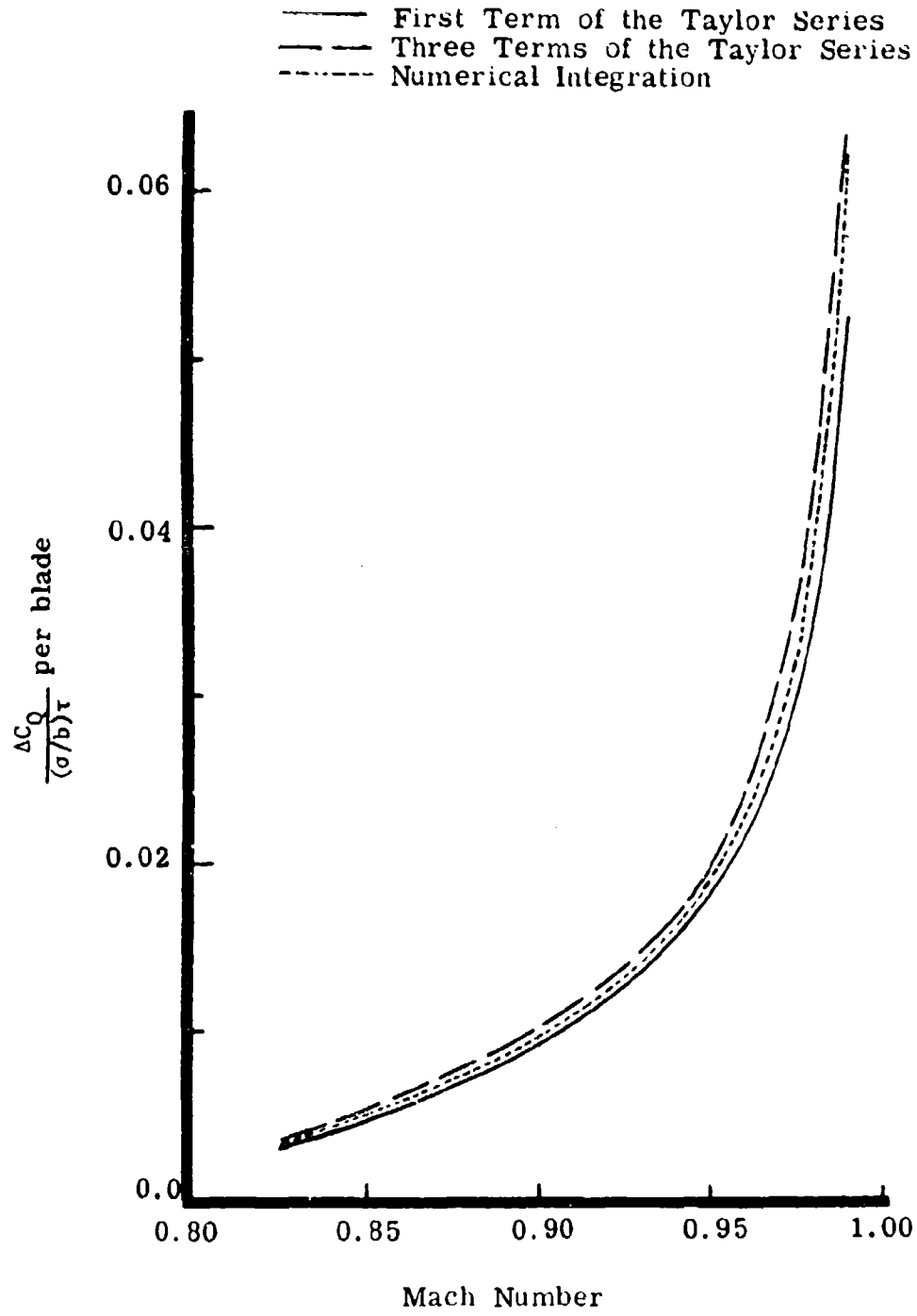

Figure 14. Change in Torque Coefficient Due to Tip Relief for a Hovering Rotor ($\sigma/b = 0.0159$). (Note Displaced Origin.)

The change in torque varies drastically with tip Mach number, and increases rapidly as Mach one is approached. This is due to the use of the compressible flow transformations discussed on page 50. All of these transformations behave in a manner similar to the Prandtl-Glauert transformation, having an infinite singularity at Mach number equal to one. The results presented here used the Prandtl-Glauert transformation, although for application, the extensions of the Prandtl-Glauert transformation that were discussed should be investigated.

The change in torque coefficient divided by solidity per blade due to tip relief at two different solidities is shown in Figure 15. Solidity of 0.0159 per blade corresponds to a blade of aspect ratio 20, while the solidity per blade of 0.0234 represents the two-bladed UH-1F helicopter. The quantity $\Delta C_Q/(\sigma/b)$ increases with solidity. This is as expected; with the greater amount of blade area, the flow is less like two dimensional.

Also indicated on Figure 15 is some comparison with test data. The data is obtained from Reference 31, Figure 9, where the measured power coefficient (numerically equal to the torque coefficient) of a UH-1F helicopter at $\mu = 0.25$ is presented along with the predicted performance based on Tanner.[23] The experimental value of the torque coefficient due to tip relief is the difference between these two curves.

The figure shows remarkable agreement, but because of the difference in conditions used for the two cases, care must be taken in interpreting this figure. First, the difference in scale between the two figures is very large, the data being taken from a small figure. Thus, the curve indicating the test should show a wide error band. At the same maximum tip Mach number, a larger portion of a hovering rotor is in compressible flow when compared to an advancing rotor. Thus, the hovering rotor may be expected to have a larger tip relief correction than an advancing rotor at the same tip Mach number, as is indicated in Figure 15. This figure does show that the theory compares well with flight test data in both order of magnitude and trend with Mach number. Thus the theory presented here can help to explain differences between prediction and test data of helicopter rotors operating in the compressible flow regime.

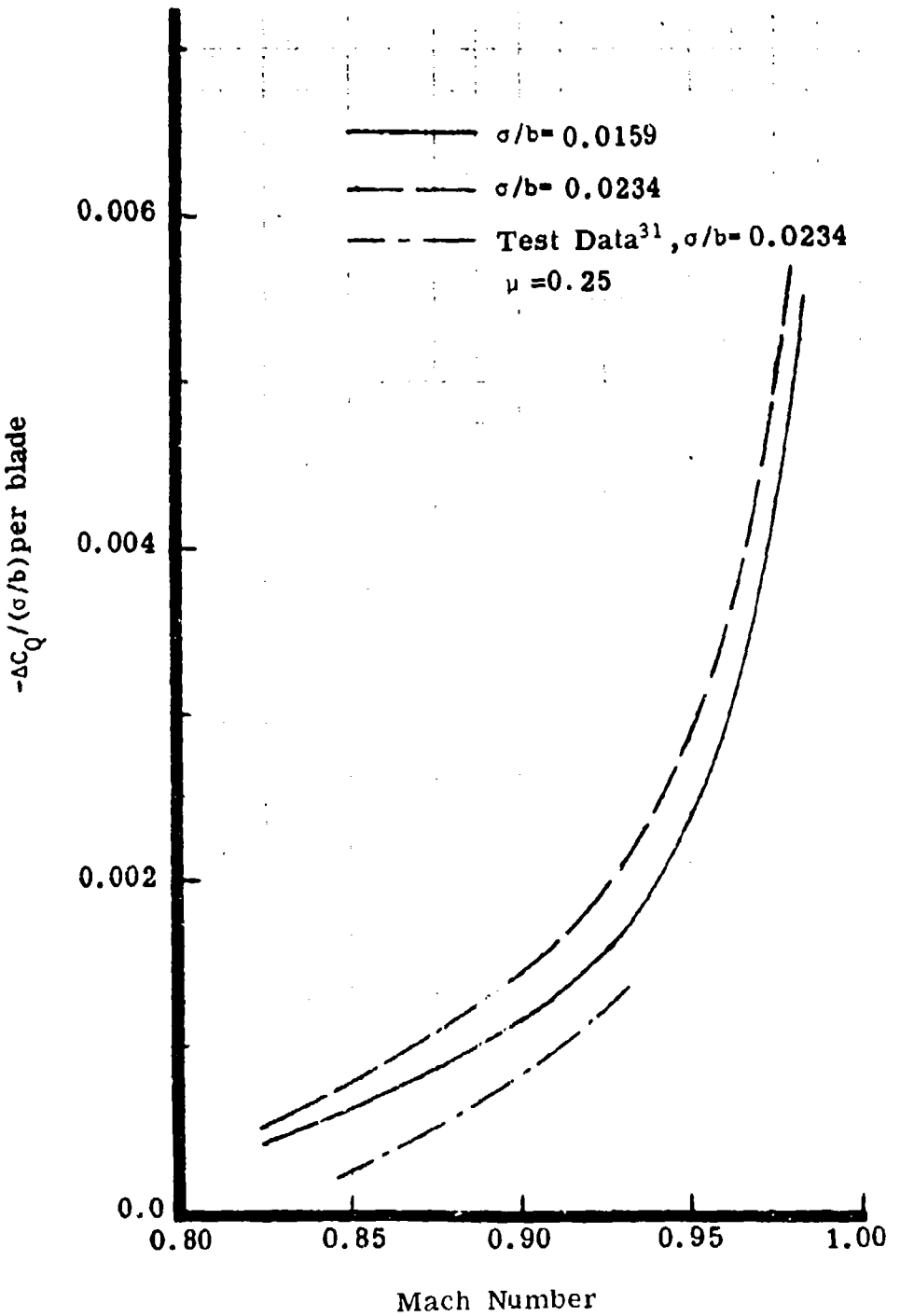

Figure 15. Change in Torque Coefficient Due to Tip Relief for a Hovering Rotor. (Note Displaced Origin.)

CONCLUSIONS

A derivation has been presented which attempts to account for differences between performance prediction and flight test data, as being due to tip relief effect. The theory is based upon the complementary wing concept and results in a correction factor to the local free-stream velocity. Small perturbation theory for rotors in compressible flow is discussed to show how a Prandtl-Glauert type transformation may be used in rotary-wing theory. Application of the correction factor with the Prandtl-Glauert type transformation in blade element analysis is discussed. The use of the theory in a simplified blade element analysis results in a change in torque due to tip relief, which is compared with data.

Results from the simplified analysis are of the same order of magnitude as the discrepancy in test data, and indicate the same trend with increasing tip Mach number.

To fully exploit the theory, it should be made a part of a performance computer program using blade element analysis. By doing so, more meaningful comparison with flight test data may be made.

The tip effect is only one of the factors which influence the compressible flow over helicopter rotors. Therefore, the quantitative analysis presented in this report cannot by itself lead to a complete understanding of the performance of helicopter rotors in compressible flow.

LITERATURE CITED

1. Anderson, Gordon F., ASPECT RATIO INFLUENCE AT HIGH SUBSONIC SPEEDS, Journal of Aeronautical Sciences, Vol. 23, No. 9, September 1956, pp. 874-878. Also Brown University Technical Note WT-13; Air Research and Development Command, Office of Scientific Research OSR TN-55-232, July 1955, AD 49 365.

2. Trant, James P., Jr., A SCHEME FOR OBTAINING ANALYTICAL AND EXPERIMENTAL BASIS FOR A SATISFACTORY METHOD OF CALCULATING ROTOR BLADE COMPRESSIBILITY LOSSES, U.S. Army Aviation Materiel Laboratories, Fort Eustis, Va., Draft Memo, 21 March 1967.

3. Sopher, Robert, THREE-DIMENSIONAL POTENTIAL FLOW PAST THE SURFACE OF A ROTOR BLADE, United Aircraft Corporation, Sikorsky Aircraft Division; Proceedings of the 25th Annual National Forum of the American Helicopter Society, Paper No. 324, May 1969.

4. Gessow, Alfred, and Myers, Garry C., Jr., AERODYNAMICS OF THE HELICOPTER, New York, republished by Frederick Ungar Publishing Co., 1967.

5. Harris, Franklin D., Tazanin, Frank J., Jr., and Fisher, Richard K., Jr., ROTOR HIGH SPEED PERFORMANCE, THEORY VS. TEST, Journal of the American Helico[illegible] Society, Vol. 15, No. 3., July 1970, pp 35-44.

6. Bellinger, E. D., ANALYTICAL INVESTIGATION OF THE EFFECTS OF BLADE FLEXIBILITY, UNSTEADY AERODYNAMICS, AND VARIABLE INFLOW ON HELICOPTER ROTOR STALL CHARACTERISTICS, United Aircraft Research Laboratories, NASA CR-1769, September 1971.

7. Crimi, Peter, DEVELOPMENT AND APPLICATION OF A METHOD FOR ANALYZING DYNAMIC STALL OF HELICOPTER ROTOR BLADES, Avco Systems Division, Presented at the Working Meeting on Dynamic Stall and Stall Flutter, Langley Research Center, NASA, July 14, 1971.

8. Glauert, H., AIRPLANE PROPELLERS, in AERODYNAMIC THEORY edited by W. F. Durand, Vol. IV., Div. L., Berlin, Julius Springer, 1935. Republished by Dover Publications, Inc., New York.

9. Goldstein, Sidney, ON THE VORTEX THEORY OF SCREW PROPELLERS, Proceedings - Royal Society of London, Vol. A123, No.792,1929, pp.440-465.

10. Landgrebe, Anton J., AN ANALYTICAL METHOD FOR PREDICTING ROTOR WAKE GEOMETRY, Journal of the American Helicopter Society, Vol. 14, No. 4, October 1969, pp. 20-32.

11. Landgrebe, Anton J., AN ANALYTICAL AND EXPERIMENTAL INVESTIGATION OF HELICOPTER ROTOR HOVER PERFORMANCE AND WAKE GEOMETRY CHARACTERISTICS, United Aircraft Corporation Research Laboratories; USAAMRDL Technical Report 71-24, Eustis Directorate, U.S. Army Air Mobility Research and Development Laboratory, Fort Eustis, Virginia, June 1971, AD 728 835.

12. Sears, W. R., POTENTIAL FLOW AROUND A ROTATING CYLINDRICAL BLADE, Journal of the Aeronautical Sciences, Vol. 17, No. 3, March 1950, pp. 184-185.

13. Goorjian, Peter M., and McCroskey, W. J., POTENTIAL FLOW AROUND A ROTATING BLADE, American Institute of Aeronautics and Astronautics Journal, Vol. 8, No. 12, December 1970, pp. 2303-4.

14. Hicks, J. C., and Nash, J. F., THE CALCULATION OF THREE-DIMENSIONAL TURBULENT BOUNDARY LAYERS ON HELICOPTER ROTORS, Lockheed-Georgia Research Laboratory, NASA CR-1845, May 1971.

15. Clark, David R., and Arnoldi, Douglas R., ROTOR BLADE BOUNDARY LAYER CALCULATION PROGRAMS, United Aircraft Corporation, Sikorsky Aircraft Division; USAAVLABS Technical Report 71-1, Eustis Directorate, U.S. Army Air Mobility Research and Development Laboratory, Fort Eustis, Virginia, March 1971, AD 723 989.

16. Vogeley, Arthur W., AXIAL MOMENTUM THEORY FOR PROPELLERS IN COMPRSSIBLE FLOW, NACA TN-2164, 1951.

17. Laitone, E. V., ACTUATOR DISC THEORY FOR COMPRESSIBLE FLOW AND SUBSONIC CORRECTION FOR PROPELLERS, Journal of Aeronautical Sciences, Vol. 20, No. 5, May 1953, pp. 365-6.

18. Delano, James B., and Crigler, John L., COMPRESSIBLE FLOW SOLUTIONS FOR THE ACTUATOR DISK, NACA RM L 53A07, March 1953.

19. Laitone, E. V., and Talbot, Lawrence, SUBSONIC COMPRESSIBILITY CORRECTIONS FOR PROPELLERS AND HELICOPTER ROTORS, Journal of Aeronautical Sciences, Vol. 20, No. 10, October 1953, pp. 683-690.

20. Head, R. M., THE EFFECT OF COMPRESSIBILITY ON THE THRUST AND POWER OF A HELICOPTER ROTOR, Douglas Aircraft Company Report No. SM-18475, August 1954, AD 196 [illegible]

21. Amer, Kenneth B., EFFECT OF BLADE STALLING AND DRAG DIVERGENCE ON POWER REQUIRED BY A HELICOPTER ROTOR AT HIGH FORWARD SPEED, Proceedings of the Eleventh Annual Forum of the American Helicopter Society, April 1955.

22. Gessow, Alfred, and Crim, Almer D., A THEORETICAL ESTIMATE OF THE EFFECTS OF COMPRESSIBILITY ON THE PERFORMANCE OF A HELICOPTER ROTOR IN VARIOUS FLIGHT CONDITIONS, NACA TN 3798, October 1956.

23. Tanner, Watson H., CHARTS FOR ESTIMATING ROTARY WING PERFORMANCE IN HOVER AND AT HIGH FORWARD SPEEDS, United Aircraft Corporation, NASA CR-114, November 1964.

24. Tanner, Watson H., TABLES FOR ESTIMATING ROTARY WING PERFORMANCE AT HIGH FORWARD SPEEDS, United Aircraft Corporation, NASA CR-115, November 1964.

25. Gustafson, F. B., THE APPLICATION OF AIRFOIL STUDIES TO HELICOPTER ROTOR DESIGN, NACA TN 1812, 1949.

26. Carpenter, Paul J., EFFECTS OF COMPRESSIBILITY ON THE PERFORMANCE OF TWO FULL-SCALE HELICOPTER ROTORS, NACA Report 1078, 1952 (Supersedes NACA TN 2277, 1951).

27. Shivers, James P., and Carpenter, Paul J., EFFECTS OF COMPRESSIBILITY ON ROTOR HOVERING PERFORMANCE AND SYNTHESIZED BLADE-SECTION CHARACTERISTICS DERIVED FROM MEASURED ROTOR PERFORMANCE OF BLADES HAVING NACA 0015 AIRFOIL TIP SECTIONS, NACA TN 4356, September 1958.

28. Carpenter, Paul J., [illegible]T AND PROFILE-DRAG CHARACTERISTICS OF AN NACA 0012 AIRFOIL S[illegible] AS DERIVED FROM MEASURED HELICOPTER-ROTOR HOVERING PERFORMANCE. [illegible]A TN 4357, September 1953.

29. Kisielowski, E., Bun[illegible]ad, R., Fissell, P., and Chinsky, I., GENERALIZED ROTOR PERFORMA[illegible], Vertol Division, The Boeing Company; USAAVLABS Technical Re[illegible]56-83, U.S. Army Aviation Materiel Laboratories, Fort [illegible]stis, [illegible]rginia, February 1967, AD 648 874.

30. Norman, David D., a[illegible], Dennis J., AN EMPIRICAL METHOD FOR CALCULATING THE POWE[illegible]D DUE TO COMPRESSIBILITY ON A SINGLE ROTOR HELICOPTER, Journal of the American Helicopter Society, Vol.10, No. 3, July 1965, pp. 30-36.

31. Norman, David C., and Somsel, John R., DETERMINATION OF HELICOPTER ROTOR BLADE COMPRESSIBILITY EFFECTS- PREDICTION VS. FLIGHT TEST, Paper No. 103, presented at the American Helicopter Society 23rd Annual National Forum, May 1967.

32. Parks, Dr. E. K., AN ANALYSIS OF HELICOPTER ROTOR BLADE COMPRESSIBILITY EFFECTS, Flight Research Branch Office Memo, Air Force Flight Test Center, Edwards Air Force Base, California, January 10, 1969.

33. Somsel, John R., DEVELOPMENT OF A DATA ANALYSIS TECHNIQUE FOR DETERMINING THE LEVEL FLIGHT PERFORMANCE OF A HELICOPTER ROTOR, Air Force Flight Test Center Technology Document No. 70-1, FTC-TD-70-1, Air Force Flight Test Center, Edwards Air Force Base, California, AD 703 719.

34. Bulban, Erwin J., BELL STRESSES EQUIPPED PROTOTYPE, Aviation Week and Space Technology, Vol. 95, No. 15, October 11, 1971, pp. 44-47.

35. Wortman, Dr. F. X., and Drees, Jan M., DESIGN OF AIRFOIL FOR ROTORS, Paper presented at the Third CAL/AVLABS Symposium on the Aerodynamics of Rotary Wing and V/STOL Aircraft, Vol. 1, June 1969.

36. Spivey, Richard F., BLADE TIP AERODYNAMICS-PROFILE AND PLANFORM EFFECTS, Paper No. 250, presented at the American Helicopter Society 24th Annual National Forum, May 1968.

37. Tanner, Watson H., and Van Wyckhouse, James F., WIND TUNNEL TESTS OF FULL SCALE ROTORS OPERATING AT HIGH ADVANCING TIP MACH NUMBERS AND ADVANCE RATIOS, Bell Helicopter Company; USAAVLABS Technical Report 68-44, U.S. Army Aviation Materiel Laboratories, Fort Eustis, Virginia, July 1968, AD 674 188.

38. Hess, R. V., and Gardner, C. S., STUDY BY THE PRANDTL-GLAUERT METHOD OF COMPRESSIBILITY EFFECTS AND CRITICAL MACH NUMBER FOR ELLIPSOIDS OF VARIOUS ASPECT RATIOS AND THICKNESS RATIOS, NACA TN 1792; Also NACA RM No. L7B03a, March 1947.

39. Shapiro, Ascher H., THE DYNAMICS AND THERMODYNAMICS OF COMPRESSIBLE FLUID FLOW, New York, The Ronald Press Company, 1953.

40. Goethert, B., EBENE UND RAUMLICHE STROMUNG BEI HOHEN UNTERSCALLGESCHWINDIGKEITEN, Lilienthal Gesellschaft Report 127, 1940. Available in English Translation as PLANE AND THREE-DIMENSIONAL FLOW AT HIGH SUBSONIC SPEEDS, NACA TM 1105, October 1946. Also available in English Translation as Ministry of Aviation, London (England) Report No. R/T 395, September 1950, AD 470 799.

41. Jones, Robert T., and Cohen, Doris, AERODYNAMICS OF WINGS AT HIGH SPEEDS, in Donovan, Allen F., and Lawrence, Herbert R., editors, AERODYNAMIC COMPONENTS OF AIRCRAFT AT HIGH SPEEDS, Volume VII of High Speed Aerodynamics and Jet Propulsion, Princeton, New Jersey Princeton University Press, 1957.

42. Petit Bois, G., TABLES OF INDEFINITE INTEGRALS, Dover Edition, New York, Dover Publications, Inc., 1964.

43. Anderson, Gordon F., and Carroll, J. B., EXPERIMENTAL INVESTIGATION OF ASPECT RATIO INFLUENCE AT HIGH SUBSONIC AND TRANSONIC SPEEDS, Brown University Technical Note WT-17: Air Research and Development Command, Office of Scientific Research, OSR TN 55-242, July 1955, AD 77 494.

44. Hughes, William F., and Gaylord, Eber W., BASIC EQUATIONS OF ENGINEERING SCIENCE, New York, Schaum Publishing Company, 1964, pp. 27-28.

45. Heaslet, Max A., and Lomax, Harvard, SUPERSONIC AND TRANSONIC SMALL DISTURBANCE THEORY, in Sears, W. R., editor, GENERAL THEORY OF HIGH SPEED AERODYNAMICS, Volume VI of High Speed Aerodynamics and Jet Propulsion, Princeton, New Jersey, Princeton University Press, 1954.

46. Simonov, L. A., and Kristianovich, S. A., INFLUENCE OF AIR COMPRESSIBILITY ON INDUCTIVE VELOCITIES OF AN AIRFOIL AND AIRSCREW, Prickladnoi Matematika i Mekhanika (USSR), Vol. VTTI, No. 2, February 1944, pp. 89-88.

47. Burns, J. C., AIRSCREWS AT SUPERSONIC FORWARD SPEEDS, The Aeronautical Quarterly, Vol. III, No. 5, May 1951, pp. 23-50.

48. Jones, W. P., and Rao, B. M., COMPRESSIBILITY EFFECTS ON OSCILLATING ROTOR BLADES IN HOVERING FLIGHT, American Institute of Aeronautics and Astronautics Journal, Vol. 8, No. 2, February 1970, pp. 321-29.

49. Sears, W. R., SMALL PERTURBATION THEORY, in Sears, W. R., editor, GENERAL THEORY OF HIGH SPEED AERODYNAMICS, Volume VI of High Speed Aerodynamics and Jet Propulsion, Princeton, New Jersey, Princeton University Press, 1954.

50. Bennett, J. A., and Goradia, S. H., METHODS FOR ANALYSIS OF TWO DIMENSIONAL AIRFOILS. Lockheed Georgia Company Report ER 8591, U.S. Army Research Office, Durham, N.C., July 1966, AD 637 603 (Addenda AD 642 750).

51. Van Dyke, Milton D., SECOND ORDER SUBSONIC AIRFOIL THEORY INCLUDING EDGE EFFECTS, NACA Report 1274, 1956.

52. Van Dyke, Milton D., SECOND ORDER SUBSONIC AIRFOIL THEORY AND ITS PRACTICAL APPLICATION, NACA TN 3390, 1955, Ad 55 950.

53. Van Dyke, Milton D., THE SIMILARITY RULES FOR SECOND ORDER SUBSONIC AND SUPERSONIC FLOW, NACA TN 3390, 1955, AD 55 950.

54. Kuchemann, D., and Weber, J., THE SUBSONIC FLOW PAST SWEPT WINGS AT ZERO LIFT WITHOUT AND WITH BODY, Ministry of Supply, Aeronautical Research Council, Reports and Memoranda No. 2908, Her Majesty's Stationery Office, London, Great Britain, March 1953.

55. Arndt, Roger E. A., and Borgman, Dean C., NOISE RADIATION FROM HELICOPTER ROTORS OPERATING AT HIGH TIP MACH NUMBERS, Journal of the American Helicopter Society, Vol. 16, No. 1, January 1971, pp. 36-45.

56. Caradona, Frank X., and Isom, Morris P., SUBSONIC AND TRANSONIC POTENTIAL FLOW OVER HELICOPTER ROTOR BLADES, AIAA Paper No. 72-39, Presented at the 10th Aerospace Sciences Meeting, San Diego, California, January 17-19, 1972.